Human Molecular Genetics, 2020, Vol. 29, No. 17 2813–2830

doi: 10.1093/hmg/ddaa161
Advance Access Publication Date: 27 July 2020
General Article

GENERAL ARTICLE

Erbb4 regulates the oocyte microenvironment during folliculogenesis

Ville Veikkolainen[1], Nsrein Ali[2,†], Milena Doroszko[3,4,†], Antti Kiviniemi[2], Ilkka Miinalainen[5], Claes Ohlsson[6], Matti Poutanen[3,6], Nafis Rahman[3], Klaus Elenius[1,7], Seppo J. Vainio[4,8] and Florence Naillat[2,*]

[1]Institute of Biomedicine and MediCity Research Laboratory, University of Turku, FI-20520 Turku, Finland, [2]Organogenesis Laboratory, Department of Medical Biochemistry and Molecular Biology, Biocenter Oulu, University of Oulu, FI-90014 Oulu, Finland, [3]Institute of Biomedicine, Research Centre for Integrative Physiology and Pharmacology, University of Turku, FI-20520 Turku, Finland, [4]Department of Immunology Genetics and Pathology, Section for Neuro-oncology, Uppsala University, 752 36 Uppsala, Sweden, [5]Electron Microscopy Unit, Biocenter Oulu, University of Oulu, FI-90220 Oulu, Finland, [6]Institute of Medicine, Sahlgrenska Academy, University of Gothenburg, SE-41345 Gothenburg, Sweden, [7]Department of Oncology, Turku University Hospital, FI-20520 Turku, Finland and [8]InfoTech Oulu, Oulu University and Biobank Borealis of Northern Finland, Oulu University Hospital, University of Oulu, FI-90014 Oulu, Finland

*To whom correspondence should be addressed. Tel: +358-503093630; Fax: +358 8 344 084; Email: Florence.naillat@oulu.fi

Abstract

Polycystic ovary syndrome (PCOS) is one of the most common endocrine disorders leading to infertility in women affecting reproductive, endocrine and metabolic systems. Recent genomewide association studies on PCOS cohorts revealed a single nucleotide polymorphism (SNP) in the *ERBB4* receptor tyrosine kinase 4 gene, but its role in ovary development or during folliculogenesis remains poorly understood. Since no genetic animal models mimicking all PCOS reproductive features are available, we conditionally deleted *Erbb4* in murine granulosa cells (GCs) under the control of *Amh* promoter. While we have demonstrated that Erbb4 deletion displayed aberrant ovarian function by affecting the reproductive function (asynchronous oestrous cycle leading to few ovulations and subfertility) and metabolic function (obesity), their ovaries also present severe structural and functional abnormalities (impaired oocyte development). Hormone analysis revealed an up-regulation of serum luteinizing hormone, hyperandrogenism, increased production of ovarian and circulating anti-Müllerian hormone. Our data implicate that *Erbb4* deletion in GCs leads to defective intercellular junctions between the GCs and oocytes, causing changes in the expression of genes regulating the local microenvironment of the follicles. *In vitro* culture assays reducing the level of Erbb4 via shRNAs confirm that Erbb4 is essential for regulating Amh level. In conclusion, our results indicate a functional role for Erbb4 in the ovary, especially during folliculogenesis and its reduced expression plays an important role in reproductive pathophysiology, such as PCOS development.

[†]These authors contributed equally to this work.

Received: April 29, 2020. **Revised:** July 17, 2020. **Accepted:** July 17, 2020

Graphical Abstract

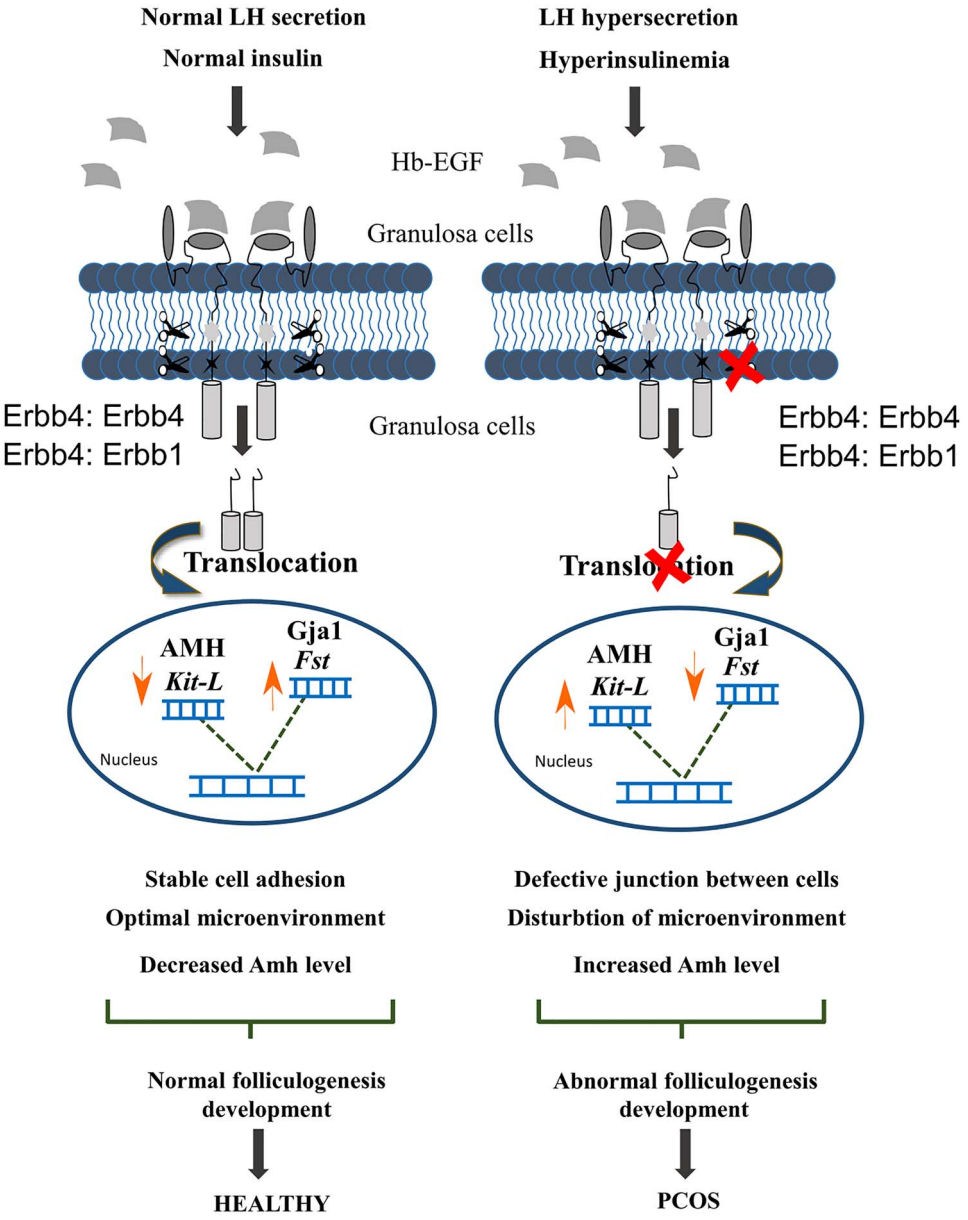

Proposed model for the mechanism by which Erbb4 may influences folliculogenesis and fertility. In healthy women, Errb4 receptor is expressed in granulosa cells (GCs), following its binding to Hb-Egf. The intracellular domain (ICD) is then translocated to the nucleus. ICD binds to the DNA to enhance or inhibit the expression of numerous genes (*Gja1*, *Fst*, *Amh* and *Kit-L*). Thus, the gene activation or inhibition results in the strong adhesion between GCs and decreased level of AMH that are required for normal follicles development. Consequently, the microenvironment and the genes expression are favourable for the normal folliculogenesis. In PCOS condition, Errb4 is significantly down-regulated resulting in non-translocated ICD signalling. As well, luteinizing hormone hypersecretion and hyperinsulinemia in the blood reinforce the dysfunction of the GCs. As consequences, Gja1 expression level is substantially decreased leading to disruption of the adhesion between the GCs as well as a significant increase of Amh hormone. Based on the unwelcoming microenvironment, the development of the follicles is not occurring properly and thus PCOS features are taking place.

Introduction

Human infertility is increasing worldwide. In Finland, for example, one woman out of six cannot become pregnant naturally and will need fertility treatment (1). A better understanding of how the signalling pathways affect and regulate fertility may provide clues for better treatment.

Dysfunction in the hypothalamo-pituitary-gonadal axis leads to reproductive disorders such as hypogonadism, amenorrhea and polycystic ovary syndrome (PCOS). PCOS is a common endocrinopathy affecting endocrine, reproductive, metabolic and psychological systems, and is the most common cause of anovulatory infertility (2). The disease is characterized by hyperandrogenism associated with ovarian dysfunction or polycystic ovaries. Furthermore, PCOS patients show an increased circulating luteinizing hormone (LH) concentration due to hyperandrogenism (3), and an increased level of anti-Müllerian hormone (AMH) due to anovulation associated with a higher number of growing follicles in the ovary (4,5). In rodent, AMH is needed to inhibit the initiation step of the recruitment of primordial follicles as well as to affect follicle stimulating hormone (FSH) sensitivity of the non-selected follicles at ovulation (6), whereas in human and non-human primates AMH does not have an action during the primordial follicle development, but its role is to promote the growth and the survival of the pre-antral follicle (AF) towards its maturation (7,8,9). Reproductive symptoms of PCOS are accompanied with life-long metabolic syndromes, such as insulin resistance, abdominal obesity, high cholesterol and blood pressure, making PCOS a health threat beyond reproductive age as well (10). According to one of the main hypotheses, the syndrome is the result of prenatal hyperandrogenic exposure that affects early embryonic development of the female offspring (11). This hypothesis has been even furthermore highlighted by Tata *et al.* (12) where excess prenatal AMH exposure alters GnRH receptor signalling in the brain of the female embryos and also inhibits aromatase expression in the placenta resulting in a reduced oestrogen level. However, the genetic and molecular mechanisms behind the development of this disease have remained poorly understood mostly because of a lack of animal models. To date, no animal models develop PCOS with all the defining characteristics of human PCOS. Consequently, examining how the PCOS syndrome develops is particularly difficult.

Two recent genome wide association studies (GWAS) of Chinese and European cohorts (13,14) have shown that a single nucleotide polymorphism (SNP) in epidermal growth factor (EGF) receptor 4 (*ERBB4*) gene is associated with PCOS, indicating its role in regulating women fertility. *Erbb4* is a member of the EGF receptor (Erbb) family, which includes *Erbb1* (also known as *Egfr*), *Erbb2*, *Erbb3* and *Erbb4*. *Erbb4* differs from the other *Erbb* genes since it can generate four alternatively spliced isoforms (JMa-CYT1, JMa-CYT2, JMb-CYT1 and JMb-CYT2) with distinct signalling properties (Fig. 1A). JM-a isoform contains a tumour necrosis factor-alpha converting enzyme (TACE) cleavage site generating an extracellular Erbb4 ectodomain whereas JMB isoform does not have it. Also, JM-a isoforms have a γ secretase that releases the soluble intracellular domain (ICD), which is translocated into the nucleus to regulate transcription (15). In mice, *Erbb4* is necessary for the development of the heart (16), kidneys (17), nervous system (18) and mammary glands (19). It is further required for proper male fertility by affecting seminiferous tubule polarity. Improper seminiferous tubule polarity may cause sperm motility defects (20) which was confirmed by a GWAS study in Japanese men (21). Expression of *Erbb4* can be observed in mouse granulosa cells (GCs) (cumulus and mural cells) during the ovulation process, and induction of ovulation by human chorionic gonadotropin (hCG), an analogue of LH, results in a decreased level of *Erbb4* expression in the ovaries of mice (22). Also, no conditional knock-out mouse line has been generated before for characterizing Erbb4 function in ovaries, we hypothesized that Erbb4 plays a key role during the selection and maturation of the oocytes.

To define how the deletion of Erbb4 in the ovary contributes to reproductive dysfunction, and to identify the molecular mechanisms that are underlying the pathophysiology, we have performed complementary *in vivo* and *in vitro* investigations, by generating a GCs conditional *Erbb4* knock-out mice and knock-down GC line to probe the role of Erbb4 in GCs. The results show that misregulated Erbb4 signalling affects ovarian function by regulating hormone and Amh production, which may cause a PCOS-like phenotype.

Results

Cleavable Erbb4 JM-a Isoforms is expressed by the GCs in the ovary

Erbb (Erbb-1, -2, -3 and -4) receptor family and its ligands are expressed in the ovaries during folliculogenesis (23); however, little is known about Erbb4 function during ovarian maturation and which ligand binds to this receptor. Quantitative RT-PCR (qPCR) revealed that *Erbb4* mRNA was expressed in the GC and oocytes of 1-month-old wild type (WT) mice whereas *Erbb4* expression is down-regulated in GCs after ovulation (GC hCG) (Fig. 1B). The *Erbb4* gene is expressed as four alternatively spliced isoforms with unique signalling characteristics (24). The isoforms are composed of alternative extracellular juxtamembrane (JM) and intracellular cytoplasmic (CYT) domains (Fig. 1A). The expression of all four Erbb4 isoforms in the 1-month-old WT ovaries was analysed by qPCR. Erbb4 expression was detected and only isoforms *JM-a CYT-1* and *JM-a CYT-2* were present, *JM-a CYT-2* was more abundant whereas *JM-b* was not observed (Fig. 1C). To confirm the cell types that express Erbb4, *in situ* hybridization and immunohistochemistry methods were carried out. In accordance with qPCR data (Fig. 1C), Erbb4 expression was detected in GCs from primary to antral follicles (AFs) (Fig. 1D, E). It is worth mentioning that only the ErbB4 JM-a isoforms can be proteolytically cleaved to produce a soluble ICD that can translocate into the nucleus and regulate transcription (25). Indeed, both nuclear and cell membrane immunostaining for ErbB4 was observed in the GCs (Fig. 1F, insert higher magnification of GCs, black arrowheads depict the nuclear staining). Taken together, these findings demonstrate that cleavable Erbb4 isoforms are expressed during folliculogenesis. Several ligands (Neuregulin, Nrg1–4; betacellulin, Btc; Heparin-binding EGF-like growth factor, Hb-Egf; Epiregulin, Ereg) bind to Erbb4 receptor to activate different pathways. We determined which potential ligand binds to Erbb4 in GCs by quantifying their mRNA expression levels. GCs expressed *Nrg1*, *Nrg4* and *Hb-EGF*, whereas cumulus cells from superovulated mice expressed *Ereg*; however, the expression of *Btc* was observed in both conditions (Fig. 1G). Altogether, our data demonstrate that GCs express Erbb4 specifically *JM-a* isoform and Erbb4 interacts with selective receptors depending on the ovarian cycle suggesting an important function in the ovaries.

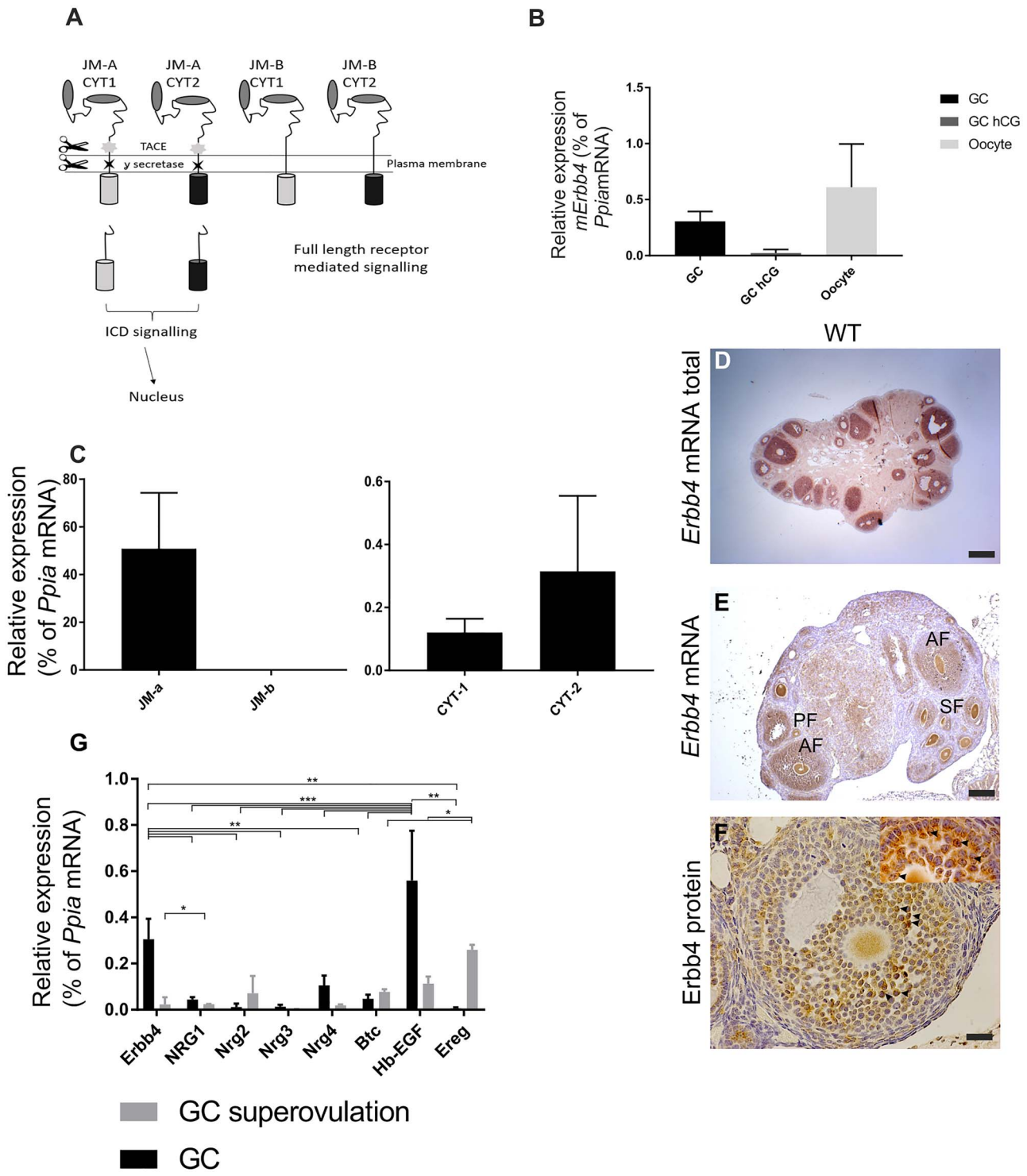

Figure 1. Erbb4 expression in the ovary. (**A**) Alternative splicing generates four Erbb4 isoforms that differ at the extracellular JM or the CYT domains. Tumour necrosis factor-α-converting enzyme (TACE) and γ-secretase cleave JM-a isoforms to produce a soluble ICD capable of translocating to the nucleus and regulating transcription. CYT-2 isoforms differ from CYT-1 isoforms by lacking 16 amino acids known to include a PI3-K binding site and a proline-rich interaction motif for WW domain-containing proteins. (**B**) Expression of the *Erbb4* mRNA in WT GCs, superovulated GCs (hCG) and oocytes. (**C**) Expression of transcripts encoding all four *Erbb4* isoforms was analysed at 1-month-old ovaries by real-time qPCR. *Ppia* was used as a reference gene to normalize expression levels. (**D–E**) *In situ* hybridization analysis of *Erbb4* in 2-month-old mouse ovaries demonstrated expression in the GCs. (**F**) Immunohistochemical analysis of ErbB4 expression in 17 days old mouse ovary demonstrated expression in the GCs from primary to pre-AFs consistent with the *in situ* hybridization analysis. Higher magnification of AF stained with an antibody (sc-283) recognizing the carboxy terminus of ErbB4 demonstrated nuclear immunoreactivity in GCs (black arrows). (**G**) Expression of transcripts encoding all ligands binding to Erbb4 was analysed in *in vivo* and superovulated GCs by real-time qPCR ($n = 3$). *Ppia* was used as a reference gene to normalize expression levels. Scale bars correspond to 500 µm (D, E), 50 µm (F). Bars represent means ± SD, two-way Anova; $^{*}P \leq 0.05$, $^{**}P \leq 0.01$, $^{***}P \leq 0.001$.

Erbb4 loss reduces cleavable Erbb4 JM-a CYT-2 Isoforms in the ovaries

To dissect the Erbb4 function in GCs of adult mice, we crossbred mice with floxed *Erbb4* gene ($Erbb4^{Flox}$) (26) with mice expressing *Cre* recombinase under GC-specific Müllerian inhibiting substance (*Amh*) gene (*AmhCre*) (27). We first confirmed the granulosa specific expression by intercrossing *AmhCre* and *Rosa26LacZ* reporter mice (28). The results showed positive LacZ staining only in the GCs and not in the oocyte of the secondary follicle (SF) after birth (Supplementary Material, Fig. S1A). To verify whether *Erbb4* expression has not been deleted in the other tissues expressing Amh, such as uterus and pituitary glands, qPCR was carried out. *Erbb4* mRNA in the uterus and pituitary glands were not affected by *Erbb4* deletion, whereas in the ovaries *Erbb4* mRNA was reduced by three folds (Fig. 2A). The weights of both organs did not change (Supplementary Material, Fig. S2A, B) and the histology of the uterus was similar in both genotypes (Supplementary Material, Fig. S2C, D).

Immunohistochemistry indicated that Erbb4 was indeed expressed in the GCs of the primary, secondary and pre-AFs of 17 days WT females (Fig. 2B-D). However, in the GCs of $Erbb4^{Flox/Flox}$; $AmhCre^{+}$ mice at the same age, Erbb4 expression was markedly reduced in the cell membrane or in the nucleus (Fig. 2E-G) from the primary follicles (PFs) stage onward, however, its expression remained detected in the oocytes. The efficiency of the *AmhCre*-mediated recombination varied, but on average the qPCR data showed an 81% reduction of *Erbb4* expression compared to the 2-month-old WT control females (data not shown). To further confirm the immuno-histochemistry results, qPCR for *Erbb4* isoforms was carried out. As expected, *JM-a* expression was down-regulated by five folds. One fold change for *CYT-2* expression was observed in the $Erbb4^{Flox/Flox}$; $AmhCre^{+}$ ovaries, whereas *CYT-1* remained expressed (Fig. 2H, I). In $Erbb4^{Flox/Flox}$; $AmhCre^{+}$ mice, western blot analysis with ErbB4 antibody indicated a notable reduction in Erbb4 (180KD) and its cleavable intracellular domain (ICD, 80KD) in the ovaries of the $Erbb4^{Flox/Flox}$; $AmhCre^{+}$ mice (Fig. 2J) in line with the qPCR and immunostaining data. Together, the results suggest that Erbb4, JM-a CYT-1 isoform producing the cleavable ICD, is involved during ovarian development and folliculogenesis.

Reduced fertility and prolonged oestrous cycle in the $Erbb4^{Flox/Flox}$; $AmhCre^{+}$ females

To analyse the fertility of the $Erbb4^{Flox/Flox}$; $AmhCre^{+}$ females, we repeatedly bred the females with males of proven fertility. We found that $Erbb4^{Flox/Flox}$; $AmhCre^{+}$ females were subfertile having less progeny compared to the WT females, and giving birth to an average of six pups per litter compared to eight pups for the WT mice followed for 8 months ($n = 10$ for each genotypes, $P < 0.001$, Fig. 3A, Supplementary Material, Fig. S3A).

To explore if the regularity of the oestrous cycle is affected, we collected vaginal smears from $Erbb4^{Flox/Flox}$; $AmhCre^{+}$ and WT females at the age of 2, 3 and 5 months. The WT females had a regular oestrous cycle of 3–5 days, whereas the $Erbb4^{Flox/Flox}$; $AmhCre^{+}$ females had an irregular oestrous cycle ranging from 5 to 17 days with a significant decrease of time at metestrous (2–3 months old) and an increase of time at diestrous (3–5 month old) ($P < 0.05$, $n = 10$ for each genotype, Fig. 3B-D). To further investigate the changes in ovarian histology, sections of ovaries from 5-week-old to 6-month-old $Erbb4^{Flox/Flox}$; $AmhCre^{+}$ females were evaluated. The $Erbb4^{Flox/Flox}$; $AmhCre^{+}$ ovaries at P35 contained follicles with oocytes that were similar to the WT ovaries (Fig. 3E-F), but by the age of 3 and 6 months, significant differences were observed (Fig. 3G-J). To further characterize the effect of the *Erbb4* depletion in GCs on the ovarian function, follicle type counts were performed between $Erbb4^{Flox/Flox}$; $AmhCre^{+}$ and WT mice at the age of P35 and 3 months. Growing follicles are classified into four groups as primordial (oocyte surrounded by squamous GC layer), primary (oocyte surrounded by a single layer of cuboidal GCs), secondary (oocyte surrounded by several layers of GCs) and AFs (follicle with a central located antrum), whereas the last class represents the soon ovulated oocytes. Based on their morphology (29), the follicles were grouped into different categories: primordial (dormant), primary, secondary, antral (growing) and atretic (dying). At P35, the $Erbb4^{Flox/Flox}$; $AmhCre^{+}$ ovaries displayed a higher number of secondary growing follicles compared to the WT ovaries ($P < 0.05$, $n = 3$ $Erbb4^{Flox/Flox}$; $AmhCre^{+}$, $n = 3$ WT, Fig. 3K). The data gathered at the age of 3 months were in line with the P35 stage data ($P < 0.05$, $n = 7$ $Erbb4^{Flox/Flox}$; $AmhCre^{+}$, $n = 3$ WT, Fig. 3L) showing that the oocytes were kept more in the stage of SFs. The number of atretic follicles did not changed between the genotypes. Furthermore, at the age of P35 and 3 months, the $Erbb4^{Flox/Flox}$; $AmhCre^{+}$ ovaries showed very few corpora lutea ($P < 0.001$, Fig. 3F-J, K, L) which is in line with the disrupted oestrous cycle and the lack of proper ovulation. Collectively, our data demonstrate that the lack of Erbb4 reduces fertility and induces changes during the oestrous cycle, prolonging the late luteal phase.

Reduction of *Erbb4* delays ovulation by entrapping the oocytes in SF stage

As we observed an arrest of some follicles at the secondary stage, we fully characterized the follicle phenotype by histological examination at 25 days old and 3 months. The nucleus of WT follicles was condensed at both stages (Fig. 4A, D), whereas several $Erbb4^{Flox/Flox}$; $AmhCre^{+}$ oocytes showed decondensed chromatin or degenerating oocytes (Fig. 4B, C, E-I). Some of the oocytes that failed to ovulate were entrapped in luteinized GCs (Fig. 4J) suggesting that the follicle maturation and oocyte activation were not synchronized properly. Further, we examined the number of abnormal entrapped oocytes in cross-sections of ovaries from control and $Erbb4^{Flox/Flox}$; $AmhCre^{+}$ females at 3 months old. The outcomes revealed the presence of 18.8 ± 7.8 abnormal oocytes per cross-section in $Erbb4^{Flox/Flox}$; $AmhCre^{+}$ mice at 3 months old compared to 8 ± 2.5 in WT females, and normal oocytes were observed in both females ($P < 0.05$, $n = 7$ $Erbb4^{Flox/Flox}$; $AmhCre^{+}$, $n = 3$ WT, Fig. 4K).

To further understand the impaired oocyte development, oocyte and GC markers were quantified by qPCR. Growth differentiation factor 9 (*Gdf9*) was up-regulated whereas the expression of other oocyte markers Homeobox protein *NOBOX*, Spermatogenesis- and oogenesis-specific basic helix-loop-helix 1, proto-oncogene receptor tyrosine kinase (*Nobox*, *Solh1*, *c-Kit*) was reduced (Fig. 4L). Granulosa markers, kit-ligand (*Kit-L*) and follistatin (*Fst*), were affected in $Erbb4^{Flox/Flox}$; $AmhCre^{+}$ ovaries ($P < 0.05$, $n = 5$ $Erbb4^{Flox/Flox}$; $AmhCre^{+}$, $n = 5$ WT, Fig. 4L). Our results demonstrate that Erbb4 and its signalling are involved in the ovulation via regulating the oocyte activation.

Erbb4 reduction induces hyperandrogenism, LH hypersecretion and alters Cyp19a1 and Hsd3b1 expression

To further understand the underlying causes for the subfertility of the $Erbb4^{Flox/Flox}$; $AmhCre^{+}$ females, we analysed the

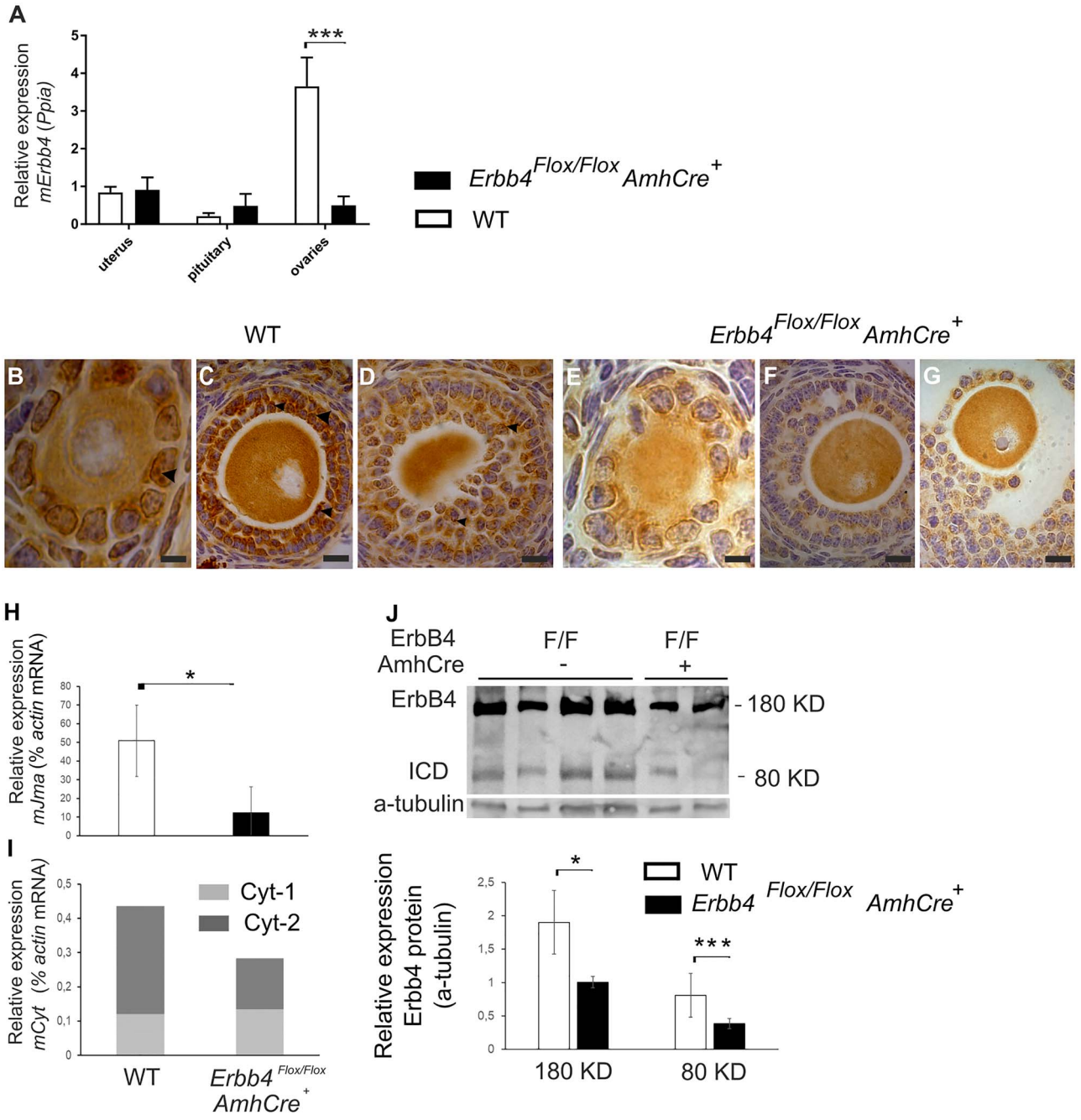

Figure 2. Conditional knockout of *Erbb4* in the GCs. (**A**) Expression of *Erbb4* transcript was analysed at 2-month-old pituitary, uterus and ovaries by real-time qPCR. (**B–G**) Immunohistochemistry of Erbb4 protein was localized in the GCs from primary to pre-AFs in WT at (**B–D**) and the expression was reduced in *Erbb4*$^{Flox/Flox}$; *AmhCre*$^{+}$ GC (**E–G**). Black arrows depict the expression of Erbb4 in the nucleus; (**H, I**) Efficiency of *AmhCre*-mediated inactivation of the floxed *Erbb4* allele by real-time qPCR of 2-month-old *Erbb4*$^{Flox/Flox}$; *AmhCre*$^{+}$ ($n = 4$, black column) and WT ovaries ($n = 4$, white column) by quantifying the isoform *JM-a*, *CYT-1* and *CYT-2*. (**J**) Western blot analyses of Erbb4 protein expression in the 3-month-old ovaries with Erbb4flox (F/F) targeted after Mis-Cre-mediated recombination (*Erbb4*$^{Flox/Flox}$; *AmhCre*$^{+}$) as compared to littermates lacking Erbb4 transgene (*Erbb4*$^{Flox/Flox}$; *AmhCre*$^{-}$). The membranes were reblotted with actin and ErbB4 to control for loading and total ErbB4 protein levels, respectively. A mean reduction of 1-fold was observed in total Erbb4 protein. Columns represent total Erbb4 Western levels (expression of full-length 180 kD receptor plus the 80 kD processed fragment, ICD) quantified by densitometry. Scale bar correspond to 20 µm (B–G). Bars represent means ± SD, 2-tailed Student's t-test; $^{*}P \leq 0.05$, $^{***}P \leq 0.001$.

serum hormone concentrations of 3-month-old mice during different phases of the oestrous cycle (proestrous, estrous and metestrous) using gas chromatography-mass spectrometry. The *Erbb4*$^{Flox/Flox}$; *AmhCre*$^{+}$ females displayed significantly irregular level of hormones during the oestrous cycle compared to the WT females (30). Serum androstenedione level is rising from oestrous to metestrus in WT ($P < 0.05$, $n = 3$ WT, two-way Anova followed by Tukey's multiple comparisons test to compare the phases of the estrous cycle within the group) whereas in the *Erbb4*$^{Flox/Flox}$; *AmhCre*$^{+}$ females the level was not increasing (Fig. 5A). Serum progesterone level increased steadily from proestrus to metestrus in WT females ($P < 0.05$, $n = 3$

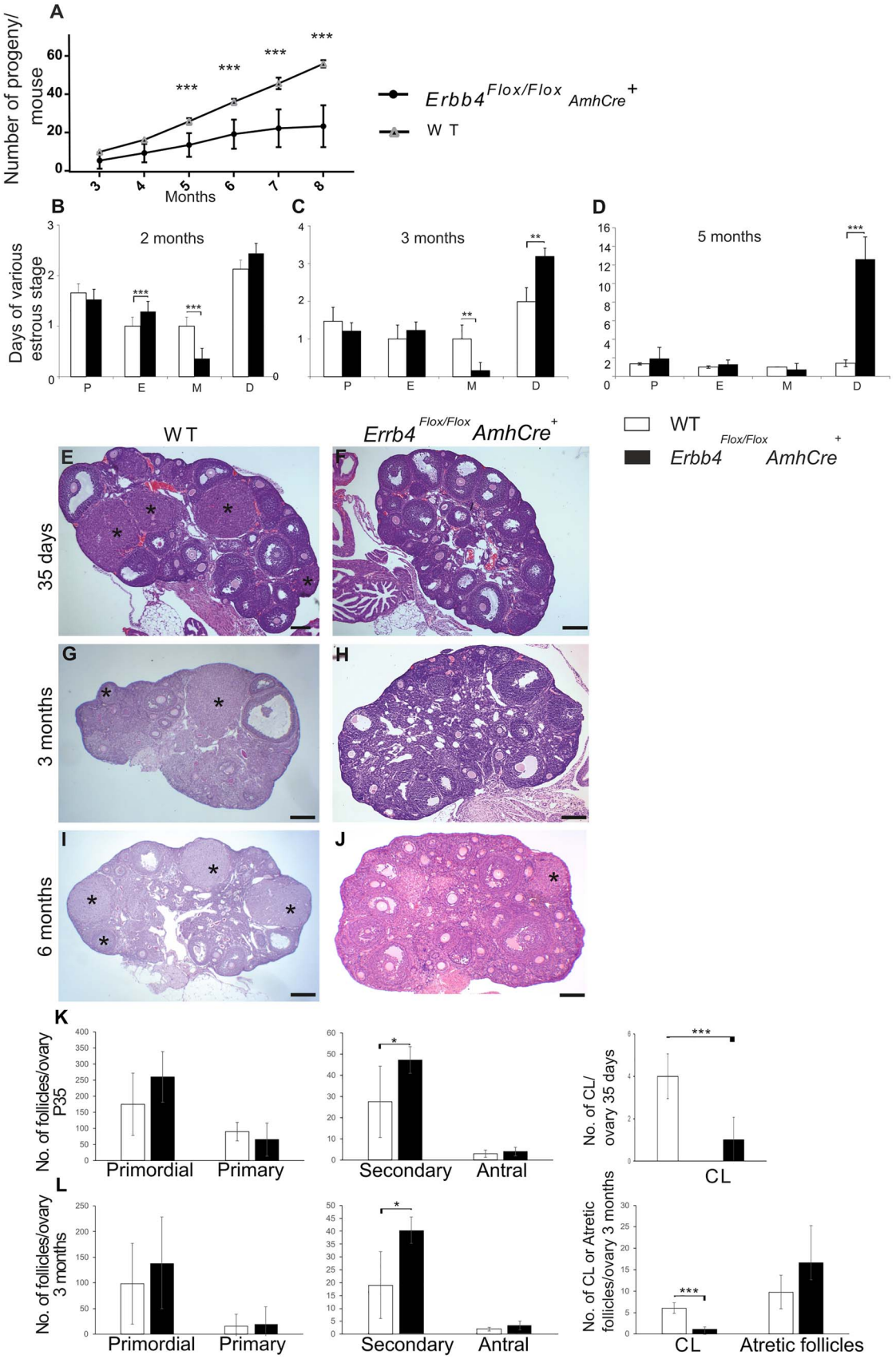

Figure 3. Ovulation is impaired in *Erbb4*$^{Flox/Flox}$; *AmhCre*$^{+}$ mice affecting fertility. (**A**) Number of progenies per mouse ($n = 10$ females from each genotype were mated). (**B–D**) Oestrous cycle of females aged 2, 3 and 5 months *Erbb4*$^{Flox/Flox}$; *AmhCre*$^{+}$ ($n = 7$, black column) and WT ($n = 7$, white column) ovaries. (**E–J**) Histological sections of 35 days, 3 and 6-month-old WT and *Erbb4*$^{Flox/Flox}$; *AmhCre*$^{+}$ ovaries. (**K**) Follicle counts at 35 days and (**L**) at 3 months in *Erbb4*$^{Flox/Flox}$; *AmhCre*$^{+}$ mice ($n = 7$, black column) and WT ($n = 3$, white column). Number of CL and atretic follicles (as depicted in Fig. 3E-J) in WT and *Erbb4*$^{Flox/Flox}$; *AmhCre*$^{+}$ mice. Scale bar corresponds to 500 µm (E–J) . Bars represent means ± SD, two-way Anova; $^{*}P \leq 0.05$, $^{**}P \leq 0.05$, $^{***}P \leq 0.001$.

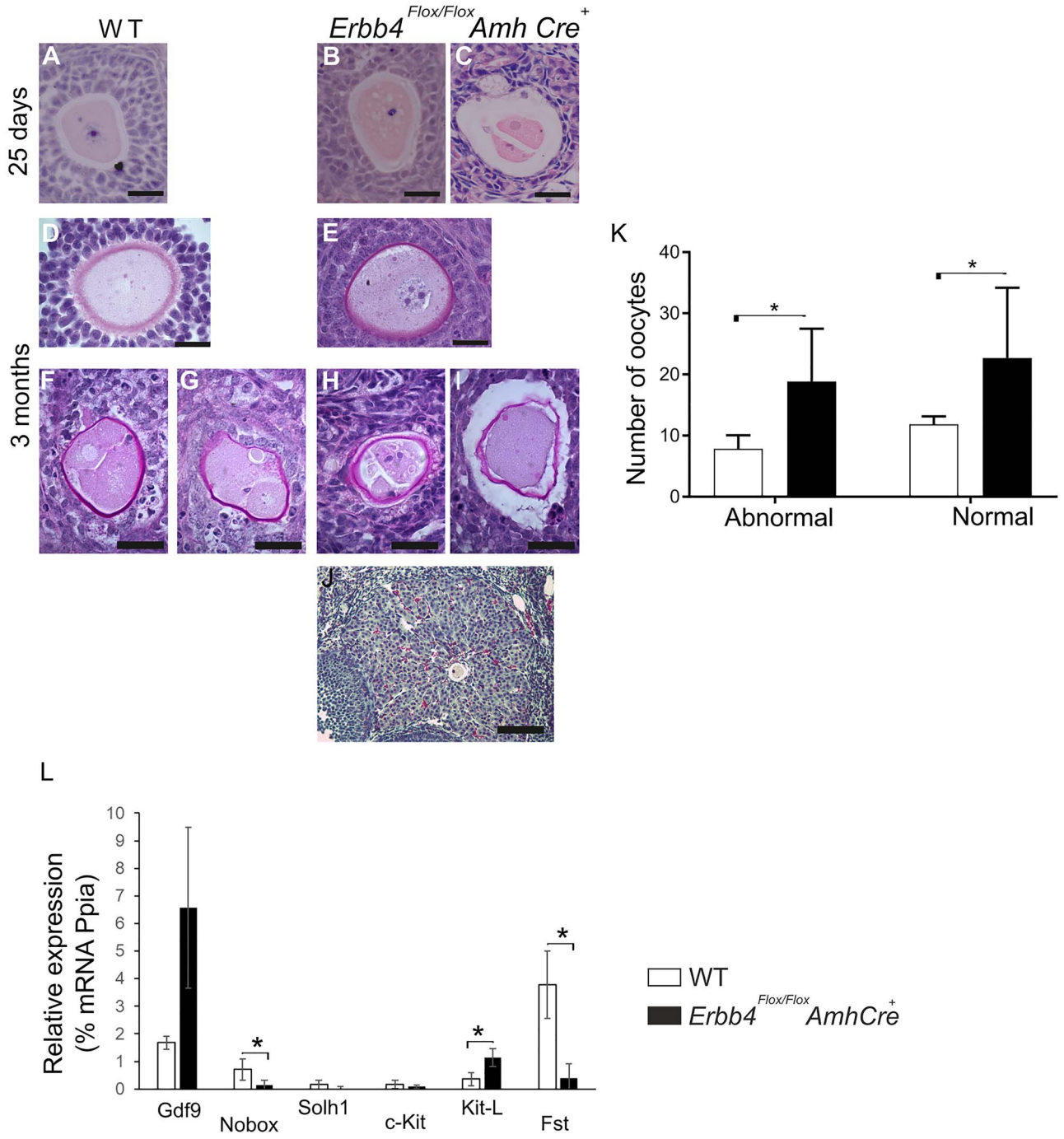

Figure 4. Oocyte failed to ovulate in *Erbb4*$^{Flox/Flox}$; *AmhCre*$^{+}$ SFs. (**A**-**J**) Higher magnification of WT oocytes (**A**, **D**). Higher magnifications showing oocyte defects that have condensed cytoplasmic fragmentation (**B**, **H**), chromatin (**E**) or are undergoing breaking (**C**, **F**–**H**), atretic oocytes (**I**) and entrapped oocyte in granulosa luteinised cells (**J**) were observed. (**K**) The number of oocytes classified as abnormal in (**E**)–(**I**) compared to normal oocytes (*Erbb4*$^{Flox/Flox}$; *AmhCre*$^{+}$ $n = 7$, black column) and WT ($n = 3$, white column) in ovarian cross-sections. (**L**) Expression of transcripts encoding oocyte (*Gdnf9*, *Nobox*, *c-Kit*, *Sohlh1*) and GC markers (*Fst*, *Kitl*) was analysed in *Erbb4*$^{Flox/Flox}$;*MisCre*$^{+}$ mice ($n = 5$) and WT ($n = 5$) 3-month-old ovaries by real-time qPCR. *Ppia* was used as a reference gene to normalize expression levels. Scale bar corresponds to 20 µm (A–I), 100 µm (J) . Bars represent means ± SD, 2-tailed Student's t-test; $^{*}P < 0.05$, $^{**}P < 0.01$.

WT, two-way Anova followed by Tukey's multiple comparisons test to compare the phases of the estrous cycle within the group), whereas in the *Erbb4*$^{Flox/Flox}$; *AmhCre*$^{+}$ females the level reduced suddenly from estrous to metestrus (Fig. 5B). The oestradiol levels in both genotypes have the same pattern (Fig. 5C). Testosterone level increased from proestrus and peaked in oestrous-metestrus in *Erbb4*$^{Flox/Flox}$; *AmhCre*$^{+}$ mice ($P < 0.05$, $n = 3$ *Erbb4*$^{Flox/Flox}$; *AmhCre*$^{+}$, two-way Anova followed by Tukey's multiple comparisons test to compare the phases of the estrous cycle within the group) whereas the opposite was observed in WT mice (Fig. 5D). The results were in line with the observed abnormal folliculogenesis and the lack of proper ovulation. Analysis of gonadotropin concentrations revealed that LH was increased in 2-, 3- and 6-month-old mice ($P < 0.05$, Fig. 5E)

and FSH was not affected compared to the age-matched WT littermates (Fig. 5F).

We also analysed the LH receptor (*Lhcgr*) mRNA localization in diestrous cycle phase ovaries. In the WT ovaries, *Lhcgr* was localized in the theca cells of the AFs and corpus luteum (CL) (Fig. 5G), whereas in the *Erbb4*$^{Flox/Flox}$; *AmhCre*$^{+}$ ovaries abundant expression was found in the mural GCs of the AFs, in the theca cells, in the CL and the interstitium (Fig. 5H).

To further analyse the biosynthesis of steroidogenic hormones in the ovary, we performed *in situ* hybridization experiments on steroidogenic enzyme genes 3 *beta-hydroxysteroid dehydrogenase* (*Hsd3b1*), *hydroxysteroid 17-beta dehydrogenase 1* (*Hsd17b1*) and *aromatase* (*Cyp19a1*). LH is a potent inducer of *Hsd3b1* mRNA in GCs during the ovulatory period (31). In the WT ovaries, *Hsd3b1* was expressed in the theca cells (arrows) and GCs (yellow arrowheads) of growing follicles (pre-antral (PA) and secondary (SF) follicles) and distributed in the functional luteal cells, CL (Fig. 5I, K). We found a reduced expression of the *Hsd3b1* gene in the *Erbb4*$^{Flox/Flox}$; *AmhCre*$^{+}$ GCs (Fig. 5J, L). Hsd17b1 is an essential enzyme for the synthesis of testosterone from androstenedione and for converting oestrone (E1) into oestradiol (E2). Cyp19a1 is the enzyme converting testosterone into E2. In the WT ovaries, *Hsd17b1* and *Cyp19a1* are expressed in the GCs of growing follicles, are down-regulated in luteinizing GCs and not present in the corpora lutea (32). As expected, the *Erbb4*$^{Flox/Flox}$; *AmhCre*$^{+}$ females also had abundant *Hsd17b1* and *Cyp19a1* transcripts in the GCs (Fig. 5M, N). Our data demonstrate that the reduction of Erbb4 induces hormone level imbalance in *Erbb4*$^{Flox/Flox}$; *AmhCre*$^{+}$ females mice.

Erbb4 reduction promotes structural changes of theca cells and disturbs cell adhesion in GCs

To understand more deeply why the follicle growth was not developing properly, we looked at the ultrastructure of AFs by electron microscopy. In the ovaries of *Erbb4*$^{Flox/Flox}$; *AmhCre*$^{+}$ females, the granulosa/cumulus cells were less connected to each other than in the ovaries of the WT mice. Increased extracellular distance was observed in the *Erbb4*$^{Flox/Flox}$; *AmhCre*$^{+}$ ovaries compared to the WT ones and the quantification was significant ($P < 0.05$, $n = 3$ *Erbb4*$^{Flox/Flox}$; *AmhCre*$^{+}$, $n = 3$ WT, Fig. 6A-C, E,G). The theca cell layer in the *Erbb4*$^{Flox/Flox}$; *AmhCre*$^{+}$ females was thicker and the theca cells contained more intracyt vesicles than in the WT ovaries ($P < 0.05$, $n = 3$ *Erbb4*$^{Flox/Flox}$; *AmhCre*$^{+}$, $n = 3$ WT, Fig. 6D-F, H). Finally, a closer look was taken to check the oocytes at the transzonal projections (TZPs) and microvilli. TZPs consist of GC extensions to reach another GCs, and microvilli are extension from the zona pellucida of the oocyte terminating on the opposite cumulus cells. TZP enable the formation of the intercellular gap junctions between the GCs required for follicular development (33). Both were reduced in *Erbb4*$^{Flox/Flox}$; *AmhCre*$^{+}$ females compared to the WT females (Fig. 7I, J; red arrowheads for TZP and black arrows for microvilli).

We further examined the cell adhesion markers for the GCs in the *Erbb4*$^{Flox/Flox}$; *AmhCre*$^{+}$ ovaries by analysing the expression of collagen IV and Connexin 43 (Gja1 or Cnx43) with immunohistochemistry. Type IV collagen (Col4A1) was localized in the theca cells, around the mature follicles in the WTs (Supplementary Material, Fig. S4A), as previously published (34), but in the *Erbb4*$^{Flox/Flox}$; *AmhCre*$^{+}$ oocytes Col4A1 expression was reduced (Supplementary Material, Fig. S4B). Gja1, a marker for gap junctions between GCs, is crucial for proper folliculogenesis, and absence or decrease of Gja1 expression in the follicle leads to impaired fertility by arresting the follicle into the early preantral stage (35). Also, gap junction marker Gja1 expression was reduced in the *Erbb4*$^{Flox/Flox}$; *AmhCre*$^{+}$ follicles (Supplementary Material, Fig. S4D compared to the WT follicles, Supplementary Material, Fig. S4C). β-catenin (Ctnnb1) is involved in mediating intercellular junctions and is predominantly expressed in the plasma membrane of GCs and zona pellucida (36). While β-catenin was mainly expressed in the GCs and zona pellucida of the WT mice, the expression pattern was expanded to cover most of the GCs and the surfaces of their plasma membrane in the *Erbb4*$^{Flox/Flox}$; *AmhCre*$^{+}$ follicles (Supplementary Material, Fig. S4E, F). These results show that the reduction of Erbb4 alters the theca cell ultrastructure and affects the adhesion between the oocyte and GCs.

Erbb4 reduction promotes obesity and adipocyte hypertrophy

A body weight comparison showed that the *Erbb4*$^{Flox/Flox}$; *AmhCre*$^{+}$ females increased than the WT control females starting from 6 weeks until the age of 6 months ($P < 0.05$; 6 weeks $n = 11$ *Erbb4*$^{Flox/Flox}$; *AmhCre*$^{+}$, $n = 10$ WT; 3 months $n = 10$ *Erbb4*$^{Flox/Flox}$; *AmhCre*$^{+}$, $n = 10$ WT; 6 months $n = 36$ *Erbb4*$^{Flox/Flox}$; *AmhCre*$^{+}$, $n = 31$ WT, Fig. 7A). In contrast, the *Erbb4*$^{Flox/Flox}$; *AmhCre*$^{+}$ females had an increased ovarian weight compared to the age-matched WT females at the age of 6 weeks and 6 months (6 weeks and 6 months $P < 0.05$; 6 weeks $n = 9$ *Erbb4*$^{Flox/Flox}$; *AmhCre*$^{+}$, $n = 10$ WT; and 6 months $n = 36$ *Erbb4*$^{Flox/Flox}$; *AmhCre*$^{+}$, $n = 31$ WT, Fig. 7B). The ratio of ovarian weight to bodyweight of *Erbb4*$^{Flox/Flox}$; *AmhCre*$^{+}$ confirmed that the ovarian weight was heavier than in WT females ($P < 0.001$ at 6 weeks $n = 9$ *Erbb4*$^{Flox/Flox}$; *AmhCre*$^{+}$, $n = 10$ WT; and $P < 0.05$ at 6 months $n = 36$ *Erbb4*$^{Flox/Flox}$; *AmhCre*$^{+}$, $n = 31$ WT, Fig. 7C).

As the Erbb4$^{Flox/Flox}$; AmhCre^{+} female mice increased their weight, we investigated the effect of *Erbb4* knockout on serum insulin levels and adipose tissue. We analysed the basal non-fasting insulin serum levels at the age of 3 months in the *Erbb4*$^{Flox/Flox}$; *AmhCre*$^{+}$ and WT females. The *Erbb4*$^{Flox/Flox}$; *AmhCre*$^{+}$ mice presented a significantly higher basal non-fasting insulin concentration than the WT females ($P < 0.05$, Fig. 7D). As *Erbb4*$^{Flox/Flox}$; *AmhCre*$^{+}$ mice presented a slightly higher body mass (Fig. 7B), gonadal adipose tissues from *Erbb4*$^{Flox/Flox}$; *AmhCre*$^{+}$ and WT females were stained with haematoxylin and eosin, and the adipocyte diameter was measured. A slight increase in the adipocyte diameter was observed but the leptin level remained the same (Fig. 7E-G, and Supplementary Material, Table S1). Altogether, our data indicate that the reduction of Erbb4 may alter the metabolic functions in female mice.

Reduction of Erbb4 signalling enhances production of intrafollicular and circulating *Amh*

Women with PCOS have elevated circulating and intrafollicular AMH levels related to an increase in the number of follicles and from hypersecretion by GCs (37). We analysed *Amh* mRNA expression by qPCR and *in situ* hybridization in the *Erbb4*$^{Flox/Flox}$; *AmhCre*$^{+}$ and WT ovaries. *Amh* expression was up-regulated significantly ($P < 0.05$, Fig. 8A) in the *Erbb4*$^{Flox/Flox}$ *MisCre*$^{+}$ ovaries compared to the WT, while its receptor *Amhr* expression remained unchanged (Fig. 8A). *In situ* hybridization on the ovaries of 3- and 6-month-old mice revealed *Amh* expression in the primary to the early AFs of both mice, but in the *Erbb4*$^{Flox/Flox}$ *AmhCre*$^{+}$ females the abundance and number of follicles expressing *Amh* was higher than in the WT (Fig. 8B-E). To follow-up on these results, we then measured the circulating

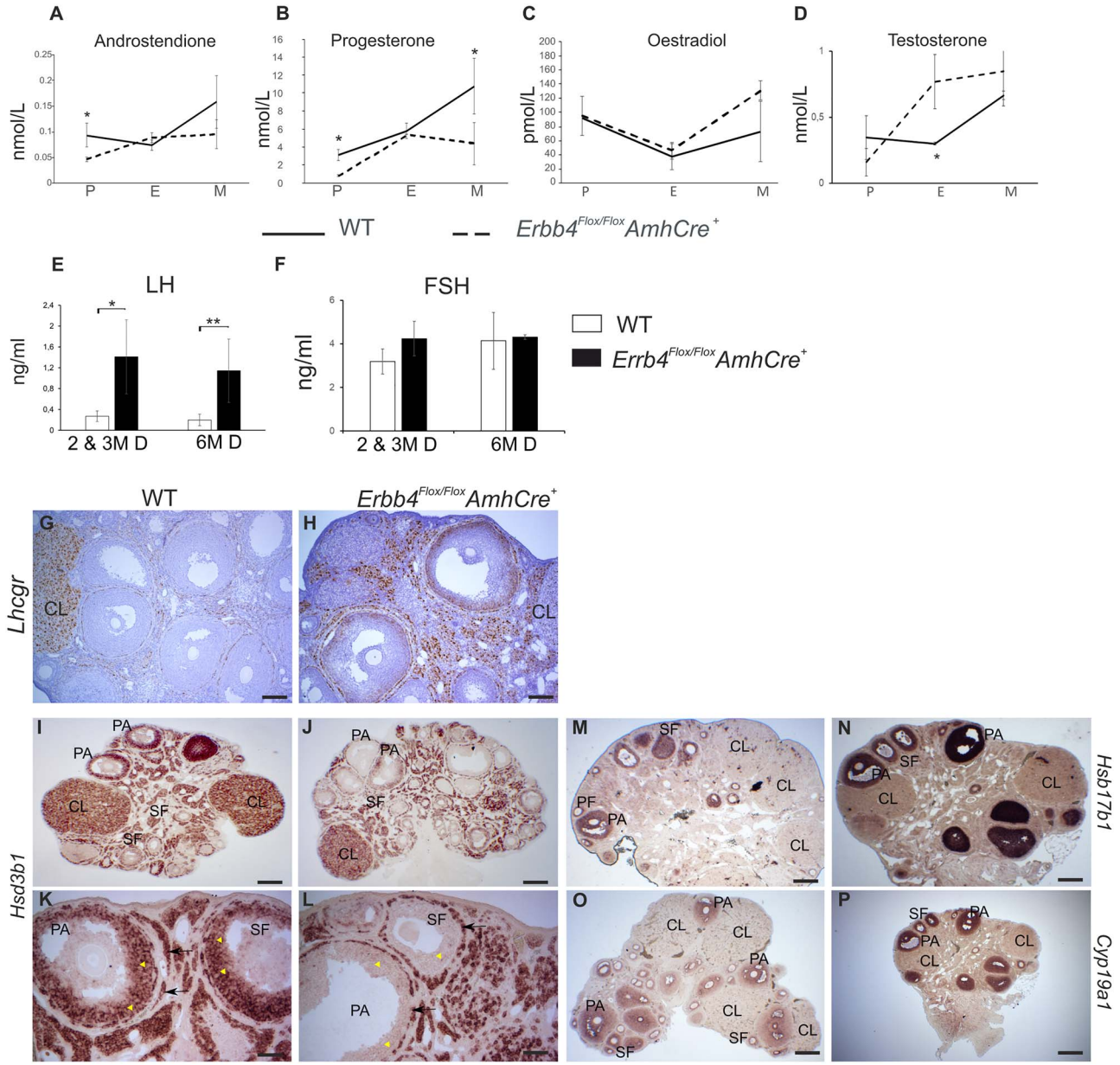

Figure 5. Hyperandrogenism and LH hypersecretion are observed in *Erbb4*$^{Flox/Flox}$*; AmhCre*$^{+}$ mice. **(A–D)** Hormone levels of androstenedione, progesterone, oestradiol and testosterone measured during the oestrous cycle (proetrous (P); estrous (E) and metestrous (M)) at the age of 3 months. **(E, F)** LH and FSH measured at diuestrus (D) for 2-, 3- and 6-months-old females. **(G, H)** *LhcgR* RNAscope *in situ* hybridization of 3-month-old WT and *Erbb4*$^{Flox/Flox}$*; AmhCre*$^{+}$ ovaries at diestrus stage. **(I–P)** *Hsd3b1, Hsd17b3, Cyp19a1 in situ* hybridization (brown colour) of 3-month-old WT and *Erbb4*$^{Flox/Flox}$*; AmhCre*$^{+}$ ovaries. Arrows show the theca cells whereas the yellow arrowheads show GCs. Scale bar corresponds to 500 µm (I, J, M–P), 100 µm (G, H, K, L). Bars represent means ± SD, 2-tailed Student's t-test; * $P < 0.05$, ** $P < 0.01$.

Amh levels. *Erbb4*$^{Flox/Flox}$ *AmhCre*$^{+}$ mice showed higher serum *Amh* levels compared to the WT mice ($P < 0.05$ at 3 months $n = 4$ for each genotype, and $P < 0.001$ at 6–8 months $n = 4$ for each genotype, Fig. 8F).

To further investigate the molecular mechanism underlying the effect of the loss of *Erbb4* in our mouse model, we took advantage of KK1 mouse GC line (35) to analyse further how Erbb4 signalling might affect Amh expression in GCs. To achieve the down-regulation of *Erbb4* in KK1 cell line, we used lentivirus (shRNAs) against mouse *Erbb4*. Erbb4 full length protein and ICD were produced in KK1 non-transfected GCs and in transfected GCs with scramble shRNA and Erbb4sh2, whereas in transfected GCs with sh1 and sh3 Erbb4 both full-length protein and ICD were down-regulated. For further analysis, we will focus only Erbb4-sh1 and -sh3 (Fig. 8G). Our data showed that Amh was up-regulated in both the ovary and in the serum of *Erbb4*$^{Flox/Flox}$*; AmhCre*$^{+}$ mice (Fig. 8A, F), we further used the same set-up to analyse the role of Erbb4 in the regulation of Amh. Also, based on the results obtained from *in vivo* GCs (Fig. 1G), demonstrating that *Hb-Egf* mRNA was more expressed in GCs than in cumulus cell and since Hb-Egf is known to be one of the ligand for Erbb4 receptors, we then examined the addition of Hb-Egf on the KK1 cell line. When Hb-Egf was added to the cell cultures, *Amh* mRNA was up-regulated in KK1 cell line transfected by Erbb4-sh3 compared to the non-treated ones ($P < 0.001$, Fig. 8H) suggesting the crosslink between Erbb4 and Amh via Hb-Egf. Collectively, this

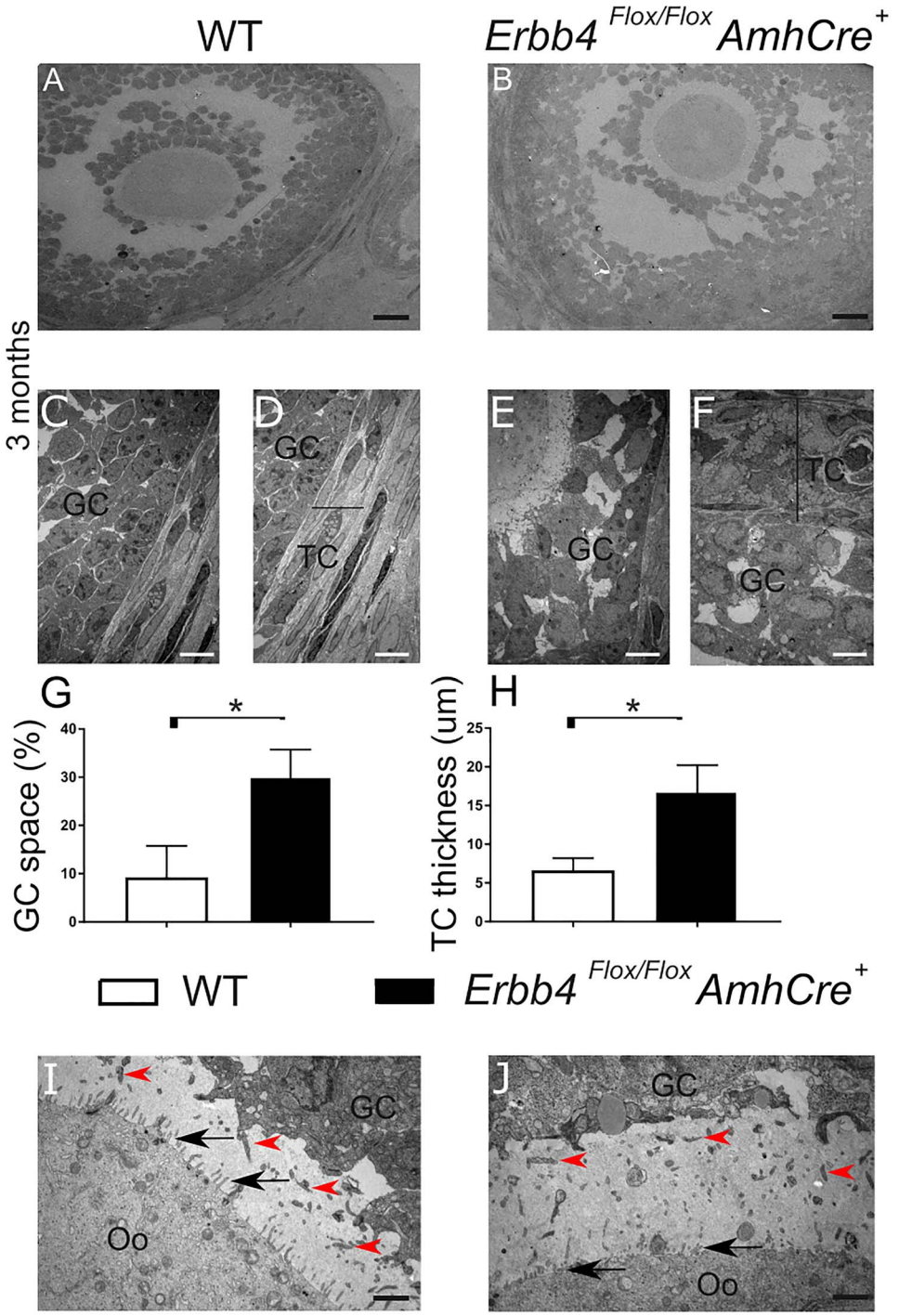

Figure 6. The thickness of theca cells layer in *Erbb4*$^{Flox/Flox}$; *AmhCre*$^{+}$ mice. (**A–F**) Electron microscopy images of the WT ($n = 3$) and *Erbb4*$^{Flox/Flox}$; *AmhCre*$^{+}$ ($n = 3$) ovaries of 3-month-old mice. (**C–F**) Higher magnification of granulosa and theca cells. (**G**) Quantification of the GC space. (**H**) Quantification of theca cells layer around the follicles. (**I, J**) Higher magnification of the transzonal processes (TZPs, red arrows) between GCs and microvilli between GCs and oocyte (black arrows) from the same follicles shown in (A) and (B). GC GC, Oo oocyte, TC theca cell. Scale bars correspond to 100 µm (A, B), 10 µm (C–F), 2 µm (I, J). Two-tailed Student's t-test; $^{*}P \leq 0.05$.

data demonstrates that Erbb4 signalling regulates the expression of Amh in the GCs and its production into the serum.

Discussion

In human ovarian follicles, *ERBB4* is known to be expressed in the mural and cumulus GCs (38). Several key traits of PCOS are on the reproductive, endocrine and metabolic characteristics shown in different animal models but how PCOS phenotype stems is still unclear. In this study, we provide evidence that supports Erbb4 signalling as a player in the development of experimental PCOS features (Table 1). Our previous study in which we analysed *Erbb4* expression by qPCR during embryonic ovarian development until birth had shown that *Erbb4* is expressed at low

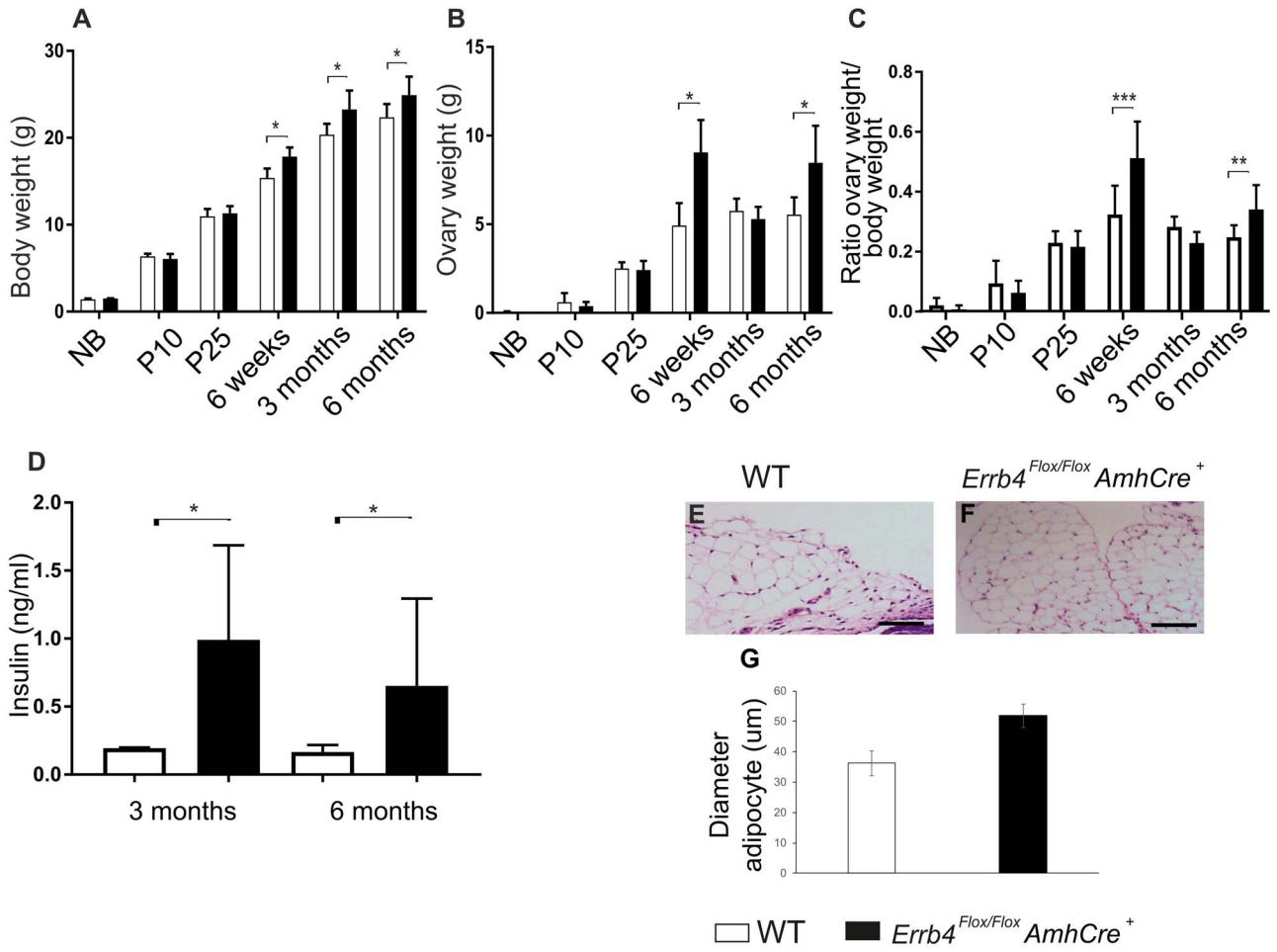

Figure 7. Obesity and metabolic changes are observed in *Erbb4*$^{Flox/Flox}$; *AmhCre*$^{+}$ mice. (**A–C**) Weights of WT and *Erbb4*$^{Flox/Flox}$; *AmhCre*$^{+}$ body and ovaries, (C) ratio of ovary weight on total body weight (*Erbb4*$^{Flox/Flox}$; *AmhCre*$^{+}$, NB $n=3$, P10 $n=10$, P25 $n=11$, 6 weeks $n=13$, 3 months $n=33$, 6 months $n=36$, black column) and WT ovaries (NB $n=5$, P10 $n=5$, P25 $n=9$, 6 weeks $n=5$, 3 months $n=30$, 6 months $n=31$ white column). NB new-born, P10 post-embryonic day 10, P25 post-embryonic day 25; (**D**) Insulin level from non-fasting WT and *Erbb4*$^{Flox/Flox}$; *AmhCre*$^{+}$ mice. (**E, F**) Haematoxylin and eosin staining of a section of gonadal adipose depots in WT ($n=3$) (A) and *Erbb4*$^{Flox/Flox}$; *AmhCre*$^{+}$ ($n=3$) at 3 months old mice. (**G**) Adipocyte diameter in *Erbb4*$^{Flox/Flox}$; *AmhCre*$^{+}$ mice ($n=3$) and WT ($n=3$) mice. Scale bar, 100 µm. Bars represent means ± SD, two-way Anova for (A) and (B), 2-tailed Student's t-test (C) and (F); *$P \leq 0.05$.

levels in embryonic ovaries (20). The current study reveals that Erbb4 expression is localized in the GCs of primary, secondary and AFs. We established a model lacking *Erbb4* gene in GCs by crossbreeding *Erbb4*$^{Flox/Flox}$ (26) with *AmhCre* (27) mice. The expression of cleavable Erbb4 isoforms JM-a CYT-1 and JM-a CYT-2 was activated in association with folliculogenesis. In the conditional *Erbb4* loss-of-function under the Amh promoter in ovaries, Erbb4 isoform JM-a CYT-2 was reduced resulting in the activity loss of the membrane-anchored ICD, whereas JM-a CYT-1 isoform was less affected. ICD translocates to the nucleus and regulates factors that activate or repress transcription (25). The observed Erbb4 expression pattern suggests that this signalling protein has a role in follicle development and the *Erbb4*$^{Flox/Flox}$ *AmhCre*$^{+}$ mice expressed several PCOS-like symptoms.

PCOS-like symptoms include infrequent or abnormal menstruation (5), increased body weight (4), a number of AFs developing large-follicle cysts increased intraovarian and circulating AMH concentrations and metabolic changes (3). In our studies, *Erbb4*$^{Flox/Flox}$; *AmhCre*$^{+}$ females showed a disturbed oestrous and a reduced number of corpora lutea, suggesting non-regular ovulation. Moreover, female total body weight was higher from P25 until the age of 6 months, associated with bigger adipocyte size, and also hyperandrogenism was observed with thickness of theca cells layer in the mutant mice. Our mouse model demonstrated an increase in the number of secondary stage follicles

Table 1. Summary of the effect of *Erbb4* deletion on the development of PCOS traits

Clinical PCOS trait[a]	*Erbb4* deletion (*Erbb4*$^{Flox/Flox}$ *AmhCre*$^{+}$)
Absent/irregular cycling	√
Oligo/anovulation	partial
Multicystic ovary	~
↑Change in ovary weight	√
↓Granulosa cell layer thickness	~
↑Theca cell layer thickness	√
↑Body weight	√
Adipocyte hypertrophy	√
↑Leptin	~
↑Insulin	√

[a]In human.
√ clinical PCOS trait present.
~ clinical PCOS trait not present.

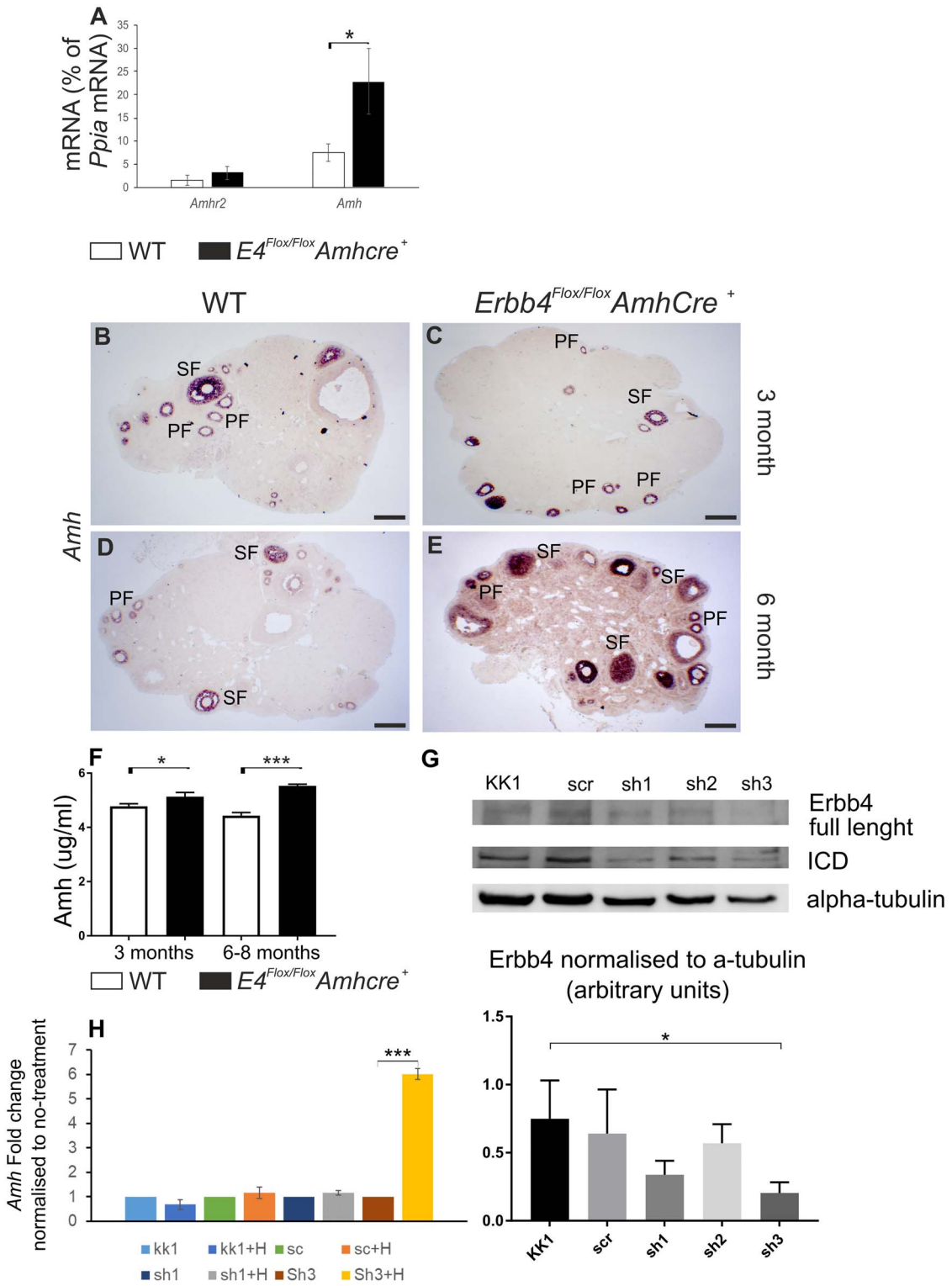

Figure 8. Amh is up-regulated in ovaries and serum from *Erbb4*$^{Flox/Flox}$; *AmhCre*$^{+}$ mice. (**A**) mRNA expression of the *Amh* and *Amhr2* in 3-month-old WT and *Erbb4*$^{Flox/Flox}$; *AmhCre*$^{+}$ ovaries. *Ppia* was used as a reference gene to normalize expression levels. (**B–E**) *Amh in situ* hybridization (brown colour) of 3 and 6-month-old WT and *Erbb4*$^{Flox/Flox}$; *AmhCre*$^{+}$ ovaries. (**F**) Circulating Amh in 3-, 6–8-months-old WT and *Erbb4*$^{Flox/Flox}$; *AmhCre*$^{+}$ mice. (**G**) Western blot analyses of Erbb4 protein expression in the transfected KK1 cell line. Sh1–3 are the shRNA against Erbb4 and scr scramble shRNA. The membranes were reblotted with alpha-tubulin and ErbB4 to control for loading and total ErbB4 protein levels, respectively. Columns represent total Erbb4. Western levels (expression of full-length 180 kD receptor plus the 80 kD processed fragment, ICD) quantified by densitometry. (**H**) Expression of transcripts encoding *Amh* was analysed by real-time qPCR in *in vitro* KK1 cell line transfected with sh1–sh3 and with or without Hb-Egf. *Ppia* was used as a reference gene to normalize expression levels. Scale bars correspond to 500 µm (B–F), Bars represent means ± SD, 2-tailed Student's t-test; $^{*}P \leq 0.05$.

in combination with increased *Amh* mRNA expression in the ovaries, as well as increased circulating Amh levels starting at the age of 3 months until the age of 6–8 months. Using an *in vitro* cell culture assay, we confirmed that a reduction of the expression of Erbb4 lead to the up-regulation of *Amh* mRNA, a similar phenotype as in the conditional knock out mice. We strongly suspect that all these characteristics in the *Erbb4*$^{Flox/Flox}$; *AmhCre*$^{+}$ females are similar to those in PCOS patients (37).

Beyond the morphological ovarian abnormalities, high levels of androgens and AMH in PCOS patients are suspected to contribute to follicle growth arrest (4). Hyperandrogenism is attributed to elevated circulating LH levels and acquisition of Lhcgr by the follicles during early stages of development (3). Growing follicles, on the other hand, secrete AMH locally, arresting their progression. This process is associated with a decreased sensitivity of the GCs to FSH (4). In *Erbb4*$^{Flox/Flox}$; *AmhCre*$^{+}$ mice, elevated LH levels increased *Lhcgr* in growing follicles and lipid content in ovarian theca cells were associated with an upregulation of *Hsd3b1* and *Hsd17b1*. The expression of both enzymes results in increased androstenedione and testosterone level. As an elevated circulating Amh concentration and mRNA content in the ovary are observed, all these results suggest a similar endocrine condition as in PCOS patients (39,40).

Tata *et al*. (12) mouse model develops PCOS-like traits due to the exposure to Amh excess during pregnancy impacting brains, ovaries and placenta of the maternal and foetal females leading to gestational hyperandrogenism with hyper-LH driving androgen hypersecretion. By comparing our developed model, we may hypothesize that our mouse model might be similar to Tata's mouse model where the female offspring might be exposed *in utero* to an excess of Amh and hyperandrogenism. Therefore, such study needs to be carried out to portray the importance of Erbb4 signalling in the establishment of PCOS-like traits.

The *Erbb4*$^{Flox/Flox}$; *AmhCre*$^{+}$ follicles presented a range of phenotypes including entrapped oocytes as early as 25 days old, which was reinforced by ultrastructure defects between GCs and oocytes (reduced TZP, microvilli and Gja1 expression). KitL is a critical factor for the growth of oocytes, and its expression level is differentially controlled by paracrine and hormonal factors. Gap junctional communications coupled GCs via Gja1 are necessary to respond to Gdnf9 and sustain KitL expression, however Gdf9 and Bmp15 influence the expression and the relative abundance of KitL during folliculogenesis (41). *Gdnf9* and *KitL* expressions were up-regulated in *Erbb4*$^{Flox/Flox}$; *AmhCre*$^{+}$ ovaries and the oocyte phenotype particularities are coinciding with a substantial reduction of TZP and microvilli in the *Erbb4*$^{Flox/Flox}$; *AmhCre*$^{+}$ females.

TZPs are the extensions of the granulosa/cumulus cell membranes that provide direct contact with the other GCs and in response oocyte membrane projects microvilli by forming adhesive and gap junctions (33). Through the gap junctions nucleic acids, proteins (42) and even lipids can be transported (43). Also, the interplay between this cargo transport and, particularly, paracrine growth factors and hormones is hypothesized to be involved in the selection, support and atresia of the follicles. It appears that the observed follicle phenotypes could be the result of the shortened connections, but why a lack of *Erbb4* affects these junctions is unclear. During the oocyte maturation phases, the number of TZPs and the proportion of adherent junctions to gap junctions fluctuates. At the final stage of oocyte maturation, the TZPs are shorter than at the beginning of the maturation process. This retraction is attributed to a surge of LH (44), so it is possible that TPZ shortening is an indirect effect of *Erbb4* knockout through elevated LH levels. Physiologically, cumulus cells do not target cells for LH action since they barely express detectable levels of Lhcgr. As a result, the involvement of paracrine factors of the mural GCs in the form of EGF-like peptides must be required. These soluble EGFs in turn function in both an autocrine and paracrine fashion to activate Erbb on theca and GCs. From these EGF-like factors Hb-EGF and Ereg which can bind to both Erbb4 and Erbb1, activate a downstream Erbb signalling pathway (24). When the Erbb pathway is activated and functional in the mural GCs, the Erbb signal is transmitted to the cumulus cells and the oocytes and plays an essential role during oocyte maturation, cumulus expansion, ovulation and luteinisation of GCs to sustain any pregnancy (45,46). Therefore, mice without functional Erbb1 in the GCs show inhibition of oocyte maturation *in vivo* and defective ovulation (45). We could hypothesize that Erbb4 and Erbb1 could work either together or separately and have different signalling pathway characteristics.

Hb-Egf interacts with either Erbb1 or Erbb4 receptor. Iwamoto *et al*. (47) show that Hb-Egf binding to Erbb4-isoform JM-a CYT-2 results in the cleavage of ICD which inhibits the valve mesenchymal cell proliferation whereas Hb-Egf binding to Erbb1 induces cell proliferation in the valves, during heart development. This example demonstrates that Hb-Egf might selectively bind to Erbb receptors. We observed that the addition of Hb-Egf in KK1 GCs transfected with sh1 or sh3 against Erbb4 did not rescue *Amh* expression. Hb-Egf needs interaction with heparan sulfate proteoglycans (HSPGs) through the heparin-binding domain of Hb-Egf. During remodelling of female reproductive organs, HSPG is reported to recruit Hb-Egf and Erbb4 (48). Combining our results and the literature, we believe that Hb-Egf recruits Erbb4 either as a homodimer Erbb4:Erbb4 or as an heterodimer Erbb1:Erbb4 in GCs for the follicle development to prepare the oocytes to be ovulated and initiated the luteinisation of GCs.

The PCOS phenotype also includes metabolic risks such as insulin resistance, abdominal obesity and high cholesterol (10). Androgen excess is associated with metabolic risk in PCOS, and patients can be divided into two categories depending on their weight: the obese and lean. Obese women with hyperandrogenism are often hyperinsulinemic, whereas lean women and hyperandrogenism might have normal or hyper-insulin secretion and sensitivity (5). Obese and lean PCOS women present alteration of intrafollicular paracrine signalling, and perturbations of the processes of follicles activation, survival, growth and selection (49). Insulin sensitivity varies by PCOS phenotype and insulin resistance is not observed in all PCOS lean and obese women (50). PCOS women, who have milder metabolic dysfunction or have a normal metabolism, might present no hyperandrogenism phenotype (51). In our studies, we found that the *Erbb4*$^{Flox/Flox}$; *AmhCre*$^{+}$ mice basal non-fasting insulin level was induced, slight body and ovary weight was increased associated with high circulating LH and lower androstenedione. We could further hypothesize that the observed results in our mouse model might be reinforced by the chronic hypoestrogenism which will affect the reduced estrous cycle frequency. If a lack of estradiol production or action is observed, such consequence will be noticed on the weight and metabolism leading to weigh gain and insulin resistance. Combining all our results, we suggest that the *Erbb4*$^{Flox/Flox}$; *AmhCre*$^{+}$ female mice present a similar phenotype as the PCOS lean women phenotype.

In conclusion, our results indicate that disruption of the *Erbb4* gene by AmhCre recombinase in female mice induces PCOS-like phenotypes. Our work provides evidence that confirms the

GWAS studies of European and Chinese cohorts that Erbb4 contributes to oocyte developmental competence, which is crucial for the proper development of an embryo.

Materials and Methods

Animals

Erbb4$^{Flox/Flox}$ (26), Rosa26LacZCre (52) and *AmhCre* (27) mice were used. To generate *Erbb4*$^{Flox/Flox}$; *AmhCre*$^{+}$ mice, *Erbb4*$^{Flox/-}$ *AmhCre*$^{+}$ heterozygote males were mated with *Erbb4*$^{Flox/Flox}$ females. The gonads of the WT littermate embryos were used as controls. All the experiments involving mice were under the Finnish national legislation, the European Convention (ETS 123), and EU Directive 86/609/EEC. Samples were collected and genotyped by PCR as previously described (26,27,52). Positive WT and *Erbb4*$^{Flox/Flox}$; *AmhCre*$^{+}$ samples were fixed in 4% paraformaldhyde (PFA) overnight at +4°C, washed in 0.1 M potassium phosphate buffer (PBS) at room temperature for 1 h, graded into 25, 50 and 75% ethanol in PBS for 2 h and stored at -20°C until processing for immunohistochemistry and *in situ* hybridization, as previously described (20).

Fertility assay, oestrous cycle assessment, histology and hormone level determination

To test fertility, single-pair matings were done between 2-month-old *Erbb4*$^{Flox/Flox}$; *AmhCre*$^{+}$ females or WT littermates and 3-month-old *Erbb4*$^{Flox/Flox}$ males. Ten matings were done for each genotype. To determine the oestrous cycle stage of the female mice, cytological analysis of the vaginal smears was performed for 20 consecutive days using seven mice for each genotype. Briefly, in the morning, the vagina of the mouse was aspirated with a drop of sterile PBS and the secretion was smeared on an objective glass. The smears were then air-dried, fixed with ethanol, stained with Mayer hematoxylin (Sigma-Aldrich, St Louis, MO, USA) and washed in tap water. The stage of the oestrous cycle was determined by analysing the cell number and type under a microscope (53).

Histology was proceed as described previously (17). The quantification of ovarian follicles was performed from consecutive histologic sections of a thickness of 7 µm from seven *Erbb4*$^{Flox/Flox}$; *AmhCre*$^{+}$ and three WT mice. The morphological classification of follicles was carried out, according to previously described staging (54), and each histologic section was compared with previous and sequential sections to prevent counting the same follicles more than once.

Blood from *Erbb4*$^{Flox/Flox}$; *AmhCre*$^{+}$ and WT littermate females was collected at the age of 2, 3, 6 and 8 months. The serum was separated by centrifugation and stored at −80°C until further analysis. FSH and LH levels were measured by immunofluorometric assays, as previously described (55). Androstenedione, progesterone, estradiol (E2) and testosterone were analysed in a single run by a validated gas chromatography tandem mass spectrometry method (30). Serum insulin levels were determined by insulin Rodent (mouse/rat) Chemiluminescence ELISA kit (ALPCO, 80-INSMR-CH01, USA), according to the manufacturer's instructions. Serum Amh levels were detected using a mouse Amh competitive ELISA kit (CUSABIO; #CSB-E13156m, USA), according to the manufacturer's protocol. Serum leptin levels were detected using a mouse/rat leptin competitive ELISA kit (ALPCO, 22-LEPMS-E01, USA), according to the manufacturer's protocol. A minimum of five serum for each stage and genotype were analysed with the selected immunoassay.

β-galactosidase staining

For β-galactosidase staining, Rosa26LacZCre ovarian tissues were immersed in a 15 and 30% sucrose solution for 15 min each, embedded in cryoMount (Leica Biosystems, Wetzlar, Germany), cut into 6 µm thick sections and stored at −80°C. Sections were air-dried for 15 min, rinsed once in PBS and fixed in 0.2% gluteraldehyde, 2mM$MgCl_2$, 5mMEGTA and 0.1 M PBS at room temperature for 1 h. After fixation, the tissues were washed with agitation in 2mM$MgCl_2$, 5 mM EGTA, 0.01% Na deoxycholate (Sigma-Aldrich, St. Louis, MO, USA), 0.02% NP-40 (Roche Applied Sciences, Indianapolis, IN, USA) and 0.01 M PBS. The tissues were stained overnight at room temperature with 10 mM $K_4Fe(CN)_6$, 10 mM $K_3Fe(CN)_6$ and 1 mg/ml X-gal (Fisher Scientific, Waltham, MA, USA). After staining, the tissues were washed, postfixed with 4% PFA, mounted with Shandon™ Immu-Mount (Fisher Scientific, New Hampshire, USA) and photographed. The experiments were carried out on 4–5 mice per group.

Immunohistochemistry

Paraffin-embedded ovaries were cut into 6 µm thick sections. Before any staining, the paraffin sections were immersed in Xylene (Sigma Pharmaceuticals, St Louis, MO, USA), washed twice in absolute ethanol and rehydrated. For histological analysis, the sections were stained with hematoxylin and eosin or with periodic acid–Schiff. For immunohistochemical analysis, antigen retrieval was performed in a pressure cooker for 20 min in 10 mmol/l citrate buffer (pH 6.0). The sections were then washed in PBS with 0.05% Tween (PBS-T), blocked with 10% goat serum (Vector Laboratories, Burlingame, CA, USA) solution in PBS for 30 min at room temperature in a humidifying chamber. After blocking, primary antibodies against goat anti-mouse Erbb4 (Errb4: sc-283, Santa Cruz), rabbit anti-mouse Connexin 43/Cnx43 (71–0700; Life Technologies, Carlsbad, CA, USA), rabbit anti-mouse Collagen IV (AB756P; Merk-Millipore, Burlington, MA, USA) and rabbit anti-mouse β-Catenin/Ctnb-1 (no. 9561; Cell Signaling Technologies, MA, USA) diluted in 1% goat serum solution in PBS-T were applied and incubated in a humidifying chamber at 4°C overnight. Samples were washed in PBS-T three times for 10 min and secondary antibodies conjugated with Alexa Fluor 488- or Alexa Fluor 546 (Invitrogen, Life Technologies, Paisley, UK) were added and incubated for 1 h at room temperature. Sections were counterstained with DAPI for 10 min at room temperature (Sigma-Aldrich, St. Louis, MO, USA). The samples were washed again and mounted in Shandon™ Immu-Mount (Fisher Scientific, NH, USA). ErbB4 immunohistochemistry was carried out, as previously described (17), except that sc-283 (1:50) (Santa Cruz Biotechnology, Santa Cruz, CA, USA) was used as the primary antibody. The slides were photographed using a confocal microscope (Olympus Fluoview FV10-ASW, Tokyo, Japan). All images were taken precisely with the same parameters for both groups. A minimum of three ovarian sections for each stage and genotype were examined with selected antibodies.

Real-time qPCR

Total RNA was extracted from collected GCs or oocytes of the 1-month-old mouse, picked up by mouth pipetting and GCs from superovulated mice using Trizol method.

The total RNA was isolated from the snap-frozen tissues of 1-month-old WT mice using the RNeasy kit (Qiagen, Venlo, The Netherlands), according to the manufacturer's instructions and dissolved in RNase-free water. The concentration of the isolated RNA was determined using Nanodrop (Fisher Scientific, USA).

The RNA samples were DNase treated with DNase I Amplification Grade Kit (Invitrogen, Thermo Fisher Scientific, USA). One hundred nanogram of the total RNA was converted into cDNA with a RevertAid First Strand cDNA Synthesis Kit (Thermo Scientific, Waltham, MA, USA) and used for real-time reverse transcription reactions.

To obtain RNA from the ovaries of 2- and 3-month-old *Erbb4*$^{Flox/Flox}$*; AmhCre*$^{+}$ and WT littermate female mice, the total RNA from sectioned paraffin ovaries was extracted using RecoverAll Total Nucleic Acid Isolation Kit (Fisher Scientific, NA, USA). The purified RNA (0.2 µg) was converted into cDNA with a RevertAid First Strand cDNA Synthesis Kit (Thermo Scientific, Waltham, MA, USA). Each qPCR reaction consisted of 2 µl of cDNA, 2.5 µM of the primers, and 5 µl of Brilliant III SYBER Green mix (Agilent Technologies) in a total volume of 10 µl. The following primers were used: *Amh*, *Amhr2*, *Fst*, *Nobox*, *Gdnf9*, *Kit, Kitl, Gapdh* (36), *Foxl2* (56), *Cre* and *Erbb4 total* and isoforms (*Jma, Jmb, Cyt-1* and *Cyt-2*) (17) and *Ppia* (57). The qPCR programme consisted of 40 cycles at 95°C for 30 s and at 60°C for 1-min run in Bio-Rad CFX96 thermocycler (Bio Rad, CA, USA). Housekeeping genes *Ppia, Gapdh* and *β-actin* were used for normalizing the data using the ΔΔCT method.

In situ hybridization

The non-radioactive *in situ* hybridization analysis of *Erbb4*, *Hsd3b1*, *Hsd17b1, Cyp19a1* and *Amh* expression was carried out, as described earlier (20). The probes for *Erbb4*, *Hsd3b1*, *Hsd17b1, Cyp19a1* and *Amh* have been described previously (36,58). A minimum of three ovary-derived sections for each genotype and stage were examined for the selected genes.

To detect *Lhcgr* transcripts, we used RNAscope® 2.5 HD Reagent Kit-BROWN (#322300, Advanced Cell Diagnostics, CA, USA) (59). The probes for *Lhcgr* (#408171, Advanced Cell Diagnostics, CA, USA), *Ppib* (positive control reference probe, #313911, Advanced Cell Diagnostics, CA, USA) and dapB (from Bacillus S., nonsense probe, #310043, Advanced Cell Diagnostics, CA, USA) were hybridized accordingly to the manufacturer's protocol. Images were taken using Leica DM4 B microscope (Leica, Wetzlar, Germany.)

Transmission electron microscopy

The dissected ovaries of 3-month-old mice ($n = 3$ for each genotype) were fixed in 1% glutaraldehyde and 4% formaldehyde in 0.1 M phosphate buffer, pH 7.4, postfixed in 1% osmium tetroxide, dehydrated in acetone and embedded in Epon LX 112 (Ladd Research Industries, USA). The semi-thin sections (1 µm) were first stained with toluidine blue for light microscopic inspection. Next, the thin sections (80 nm) were cut with a Leica Ultra cut UCT ultramicrotome, stained in uranyl acetate and lead citrate, and examined in a Tecnai Spirit G2 transmission electron microscope (FEI Company, USA). Images were captured with a Veleta CCD camera (Olympus Soft Imaging Solutions GMBH, Munster, Germany).

Western blot

The ovaries were prepared from 3-month-old mice. The proteins were purified immediately and subjected to western blotting using anti-ErbB4 (E200; Abcam), anti-α tubulin (T5168; Sigma) antibodies, as described previously (60). The bands were quantified using Image J software. The stable virus transfected cell lines were lysed using the lysis buffer, as described previously (60).

Measurement of GC, theca cell and adipocyte size

For the measurement of GC space and theca cells, signal quantification was performed using Image J software 1.52p; to measure the threshold auto-threshold was integrated to enhance the contrast between white and black. Then, the set measurement was adjusted for the area minus the corrected threshold.

Four mice per group were randomly selected, and fixed gonadal adipose tissue was processed and analysed. In brief, adipose depots were embedded in paraffin and, after routine histological preparation, sectioned at 6 µm. Mounted sections were stained with hematoxylin and eosin. The diameter of adipocytes was measured using ImageJ software.

shRNA and cell culture

KK1 cells were grown in DMEM with 10% FBS (Sigma) and 1% antibiotics. The cells were transfected with short hairpin RNA (shRNA) against mouse Erbb4 (sh41 NM_010154 TRCN0000360692; sh42 NM_010154 TRCN0000360891; sh43 NM_010154 TRCN0000360689 and scramble shRNA, Sigma). The transfected cells were selected using puromycin and stable cell lines were generated for further analyses. Cultures were supplemented with Hb-Egf (10 ng/ml, R&D System). Cell pellets were stored for either protein or RNA extraction as described above.

Statistical analysis

For comparisons between two groups, statistical significance was determined using the 2-tailed Student's t-test and for all quantitative comparisons, two-way ANOVA with Bonferroni's multiple comparisons test was performed with GraphPad Prism 7.03 software. Values of $P \leq 0.05$ and lower were considered statistically significant and the results were presented as mean standard deviation (mean ± SD). Asterisks indicate statistical significance according to this legend: $^{*}P < 0.05$: $^{**}P < 0.01$; $^{***}P < 0.001$.

Supplementary Material

Supplementary Material is available at *HMG* online.

Acknowledgments

We thank H. Härkman, J. Kekolahti-Liias, P. Haipus and A. Landin for their excellent technical assistance.

Conflict of Interest statement. None declared.

Funding

This work was supported by grants from the Academy of Finland Profiling funding to the University of Oulu Profi3 (311934); for S.J.V., by the Academy of Finland (206038, 121647, 250900, 260056), Centre of Excellence Grant 2012–2017 of the Academy of Finland (251314), and Tekes BioRealHealth (24302443); and for F.N., by the Academy of Finland post-doctoral Fellowship (243014583), the Foundations' Post Doc Pool (Svenska Kulturfonden) and the

Finnish Cultural Foundation (Pekka ja Jukka-Pekka Lylykarin rahasto).

References

1. Klemetti, R., Raitanen, J., Sihvo, S., Saarni, S. and Koponen, P. (2010) Infertility, mental disorders and well-being—a nationwide survey. *Acta Obstet. Gynecol. Scand.*, **89**, 677–682.
2. Franks, S. (1995) Polycystic ovary syndrome. *N. Engl. J. Med.*, **333**, 853–861.
3. Stubbs, S.A., Hardy, K., Da Silva-Buttkus, P., Stark, J., Webber, L.J., Flanagan, A.M., Themmen, A.P.N., Visser, J.A., Groome, N.P. and Franks, S. (2005) Anti-müllerian hormone protein expression is reduced during the initial stages of follicle development in human polycystic ovaries. *J. Clin. Endocrinol. Metab.*, **90**, 5536–5543.
4. Laven, J.S.E., Mulders, A.G.M.G.J., Visser, J.A., Themmen, A.P., De Jong, F.H. and Fauser, B.C.J.M. (2004) Anti-müllerian hormone serum concentrations in normoovulatory and anovulatory women of reproductive age. *J. Clin. Endocrinol. Metab.*, **89**, 318–323.
5. Franks, S., Stark, J. and Hardy, K. (2008) Follicle dynamics and anovulation in polycystic ovary syndrome. *Hum. Reprod. Update*, **14**, 367–378.
6. Durlinger, A.L.L., Gruijters, M.J.G., Kramer, P., Karels, B., Ingraham, H.A., Nachtigal, M.W., Uilenbroek, J.T.J., Grootegoed, J.A. and Themmen, A.P.N. (2002) Anti-müllerian hormone inhibits initiation of primordial follicle growth in the mouse ovary. *Endocrinology*, **143**, 1076–1084.
7. Rice, S., Ojha, K., Whitehead, S. and Mason, H. (2007) Stage-specific expression of androgen receptor, follicle-stimulating hormone receptor, and anti-müllerian hormone type II receptor in single, isolated, human preantral follicles: relevance to polycystic ovaries. *J. Clin. Endocrinol. Metab.*, **92**, 1034–1040.
8. Xu, J., Xu, F., Lawson, M.S., Tkachenko, O.Y., Ting, A.Y., Kahl, C.A., Park, B.S., Stouffer, R.R. and Bishop, C.V. (2018) Anti-müllerian hormone is a survival factor and promotes the growth of rhesus macaque preantral follicles during matrix-free culture. *Biol. Reprod.*, **98**, 197–207.
9. Baba, T., Ting, A.Y., Tkachenko, O., Xu, J. and Stouffer, R.L. (2017) Direct actions of androgen, estrogen and anti-müllerian hormone on primate secondary follicle development in the absence of FSH in vitro. *Hum. Reprod.*, **32**, 2456–2464.
10. Azziz, R., Carmina, E., Chen, Z., Dunaif, A., Laven, J.S.E., Legro, R.S., Lizneva, D., Natterson-Horowtiz, B., Teede, H.J. and Yildiz, B.O. (2016) Polycystic ovary syndrome. *Nat. Rev. Dis. Primers.*, **2**, 16057.
11. Filippou, P. and Homburg, R. (2017) Is foetal hyperexposure to androgens a cause of PCOS? *Hum. Reprod. Update*, **23**, 421–432.
12. Tata, B., Mimouni, N.E.H., Barbotin, A., Malone, S.A., Loyens, A., Pigny, P., Dewailly, D., Catteau-Jonard, S., Sundström-Poromaa, I., Piltonen, T.T. *et al.* (2018) Elevated prenatal anti-müllerian hormone reprograms the fetus and induces polycystic ovary syndrome in adulthood. *Nat. Med.*, **24**, 834–846.
13. Day, F.R., Hinds, D.A., Tung, J.Y., Stolk, L., Styrkarsdottir, U., Saxena, R., Bjonnes, A., Broer, L., Dunger, D.B., Halldorsson, B.V. *et al.* (2015) Causal mechanisms and balancing selection inferred from genetic associations with polycystic ovary syndrome. *Nat. Commun.*, **6**, 8464.
14. Peng, Y., Zhang, W., Yang, P., Tian, Y., Su, S., Zhang, C., Chen, Z. and Zhao, H. (2017) ERBB4 confers risk for polycystic ovary syndrome in Han Chinese. *Sci. Rep.*, **7**, 42000.
15. Elenius, K., Choi, C.J., Paul, S., Santiestevan, E., Nishi, E. and Klagsbrun, M. (1999) Characterization of a naturally occurring ErbB4 isoform that does not bind or activate phosphatidyl inositol 3-kinase. *Oncogene*, **18**, 2607–2615.
16. Tidcombe, H., Jackson-Fisher, A., Mathers, K., Stern, D.F., Gassmann, M. and Golding, J.P. (2003) Neural and mammary gland defects in ErbB4 knockout mice genetically rescued from embryonic lethality. *Proc. Natl. Acad. Sci. USA.*, **100**, 8281–8286.
17. Veikkolainen, V., Naillat, F., Railo, A., Chi, L., Manninen, A., Hohenstein, P., Hastie, N., Vainio, S. and Elenius, K. (2012) ErbB4 modulates tubular cell polarity and lumen diameter during kidney development. *J. Am. Soc. Nephrol.*, **23**, 112–122.
18. Gassmann, M., Casagranda, F., Orioli, D., Simon, H., Lai, C., Klein, R. and Lemke, G. (1995) Aberrant neural and cardiac development in mice lacking the ErbB4 neuregulin receptor. *Nature*, **378**, 390–394.
19. Jones, F.E., Welte, T., Fu, X.Y. and Stern, D.F. (1999) ErbB4 signaling in the mammary gland is required for lobuloalveolar development and Stat5 activation during lactation. *J. Cell Biol.*, **147**, 77–88.
20. Naillat, F., Veikkolainen, V., Miinalainen, I., Sipilä, P., Poutanen, M., Elenius, K. and Vainio, S.J. (2014) ErbB4, a receptor tyrosine kinase, coordinates organization of the seminiferous tubules in the developing testis. *Mol. Endocrinol.*, **28**, 1534–1546.
21. Sato, Y., Tajima, A., Sato, T., Nozawa, S., Yoshiike, M., Imoto, I., Yamauchi, A. and Iwamoto, T. (2018) *Health and Medicine—Medical Genetics; Researchers at Tokushima University Target Medical Genetics (Genome-Wide Association Study Identifies ERBB4 on 2q34 as a Novel Locus Associated with Sperm Motility in Japanese Men)*. NewsRx, Atlanta.
22. Noma, N., Kawashima, I., Fan, H., Fujita, Y., Kawai, T., Tomoda, Y., Mihara, T., Richards, J.S. and Shimada, M. (2011) LH-induced neuregulin 1 (NRG1) type III transcripts control granulosa cell differentiation and oocyte maturation. *Mol. Endocrinol.*, **25**, 104–116.
23. Conti, M., Hsieh, M., Park, J. and Su, Y. (2006) Role of the epidermal growth factor network in ovarian follicles. *Mol. Endocrinol.*, **20**, 715–723.
24. Veikkolainen, V., Vaparanta, K., Halkilahti, K., Iljin, K., Sundvall, M. and Elenius, K. (2011) Function of ERBB4 is determined by alternative splicing. *Cell Cycle*, **10**, 2647–2657.
25. Ni, C.Y., Murphy, M.P., Golde, T.E. and Carpenter, G. (2001) Gamma-secretase cleavage and nuclear localization of ErbB-4 receptor tyrosine kinase. *Science*, **294**, 2179–2181.
26. Long, W., Wagner, K.U., Lloyd, K.C., Binart, N., Shillingford, J.M., Hennighausen, L. and Jones, F.E. (2003) Impaired differentiation and lactational failure of Erbb4-deficient mammary glands identify ERBB4 as an obligate mediator of STAT5. *Development*, **130**, 5257–5268.
27. Lecureuil, C., Fontaine, I., Crepieux, P. and Guillou, F. (2002) Sertoli and granulosa cell-specific cre recombinase activity in transgenic mice. *Genesis*, **33**, 114–118.
28. Soriano, P. (1999) Generalized lacZ expression with the ROSA26 cre reporter strain. *Nat. Genet.*, **21**, 70–71.
29. Jamin, S.P., Arango, N.A., Mishina, Y., Hanks, M.C. and Behringer, R.R. (2003) Genetic studies of the AMH/MIS signaling pathway for müllerian duct regression. *Mol. Cell. Endocrinol.*, **211**, 15–19.
30. Nilsson, M.E., Vandenput, L., Tivesten, Å., Norlén, A., Lagerquist, M.K., Windahl, S.H., Börjesson, A.E., Farman, H.H., Poutanen, M., Benrick, A. *et al.* (2015) Measurement of a comprehensive sex steroid profile in rodent serum by

high-sensitive gas chromatography-tandem mass spectrometry. *Endocrinology*, **156**, 2492–2502.
31. Young, J.M. and McNeilly, A.S. (2010) Theca: the forgotten cell of the ovarian follicle. *Reproduction*, **140**, 489–504.
32. Hakkarainen, J., Jokela, H., Pakarinen, P., Heikelä, H., Kätkänaho, L., Vandenput, L., Ohlsson, C., Zhang, F. and Poutanen, M. (2015) Hydroxysteroid (17β)-dehydrogenase 1-deficient female mice present with normal puberty onset but are severely subfertile due to a defect in luteinization and progesterone production. *FASEB J.*, **29**, 3806–3816.
33. Baena, V. and Terasaki, M. (2019) Three-dimensional organization of transzonal projections and other cytoplasmic extensions in the mouse ovarian follicle. *Sci. Rep.*, **9**, 1–13.
34. Berkholtz, C.B., Lai, B.E., Woodruff, T.K. and Shea, L.D. (2006) Distribution of extracellular matrix proteins type I collagen, type IV collagen, fibronectin, and laminin in mouse folliculogenesis. *Histochem. Cell Biol.*, **126**, 583–592.
35. Winterhager, E. and Kidder, G.M. (2015) Gap junction connexins in female reproductive organs: implications for women's reproductive health. *Hum. Reprod. Update*, **21**, 340–352.
36. Prunskaite-Hyyrylainen, R., Shan, J., Railo, A., Heinonen, K.M., Miinalainen, I., Yan, W., Shen, B., Perreault, C. and Vainio, S.J. (2014) Wnt4, a pleiotropic signal for controlling cell polarity, basement membrane integrity, and antimullerian hormone expression during oocyte maturation in the female follicle. *FASEB J.*, **28**, 1568–1581.
37. Stracquadanio, M., Ciotta, L. and Palumbo, M.A. (2018) Relationship between serum anti-mullerian hormone and intrafollicular AMH levels in PCOS women. *Gynecol. Endocrinol.*, **34**, 223–228.
38. Zamah, A.M., Hsieh, M., Chen, J., Vigne, J.L., Rosen, M.P., Cedars, M.I. and Conti, M. (2010) Human oocyte maturation is dependent on LH-stimulated accumulation of the epidermal growth factor-like growth factor, amphiregulin. *Hum. Reprod.*, **25**, 2569–2578.
39. Goodarzi, M.O., Dumesic, D.A., Chazenbalk, G. and Azziz, R. (2011) Polycystic ovary syndrome: etiology, pathogenesis and diagnosis. *Nat. Rev. Endocrinol.*, **7**, 219–231.
40. Nelson, V.L., Legro, R.S., Strauss, J.F. and McAllister, J.M. (1999) Augmented androgen production is a stable steroidogenic phenotype of propagated theca cells from polycystic ovaries. *Mol. Endocrinol.*, **13**, 946–957.
41. Thomas, F.H. and Vanderhyden, B.C. (2006) Oocyte-granulosa cell interactions during mouse follicular development: regulation of kit ligand expression and its role in oocyte growth. *Reprod. Biol. Endocrinol.*, **4**, 19.
42. Albertini, D.F., Combelles, C.M., Benecchi, E. and Carabatsos, M.J. (2001) Cellular basis for paracrine regulation of ovarian follicle development. *Reproduction*, **121**, 647.
43. del Collado, M., da Silveira, J.C., Sangalli, J.R., Andrade, G.M., Sousa, L.R.d.S., Silva, L.A., Meirelles, F.V. and Perecin, F. (2017) Fatty acid binding protein 3 and transzonal projections are involved in lipid accumulation during in vitro maturation of bovine oocytes. *Sci. Rep.*, **7**, 1.
44. Suzuki, H., Jeong, B. and Yang, X. (2000) Dynamic changes of cumulus-oocyte cell communication during in vitro maturation of porcine oocytes. *Biol. Reprod.*, **63**, 723–729.
45. Hsieh, M., Lee, D., Panigone, S., Horner, K., Chen, R., Theologis, A., Lee, D.C., Threadgill, D.W. and Conti, M. (2007) Luteinizing hormone-dependent activation of the epidermal growth factor network is essential for ovulation. *Mol. Cell. Biol.*, **27**, 1914–1924.
46. Hsieh, M., Thao, K. and Conti, M. (2011) Genetic dissection of epidermal growth factor receptor signaling during luteinizing hormone-induced oocyte maturation. *PLoS One*, **6**, e21574.
47. Iwamoto, R., Mine, N., Mizushima, H. and Mekada, E. (2017) ErbB1 and ErbB4 generate opposing signals regulating mesenchymal cell proliferation during valvulogenesis. *J. Cell Sci.*, **130**, 1321–1332.
48. Yu, W., Woessner, J.F., McNeish, J.D. and Stamenkovic, I. (2002) CD44 anchors the assembly of matrilysin/MMP-7 with heparin-binding epidermal growth factor precursor and ErbB4 and regulates female reproductive organ remodeling. *Genes Dev.*, **16**, 307–323.
49. Dumesic, D.A. and Richards, J.S. (2013) Ontogeny of the ovary in polycystic ovary syndrome. *Fertil. Steril.*, **100**, 23–38.
50. Marshall, J.C. and Dunaif, A. (2012) All women with PCOS should be treated for insulin resistance. *Fertil Steril*, **97**, 18–22.
51. Barber, T.M., Wass, J.A.H., McCarthy, M.I. and Franks, S. (2007) Metabolic characteristics of women with polycystic ovaries and oligo-amenorrhoea but normal androgen levels: implications for the management of polycystic ovary syndrome. *Clin. Endocrinol.*, **66**, 513–517.
52. Jokela, T. and Vainio, S. (2007) Conditional tamoxifen cre induced mutagenesis in the embryonic kidney in organ culture. *Genesis*, **45**, 757–761.
53. Byers, S.L., Wiles, M.V., Dunn, S.L. and Taft, R.A. (2012) Mouse estrous cycle identification tool and images. *PLoS One*, **7**, e35538.
54. Myers, M., Middlebrook, B.S., Matzuk, M.M. and Pangas, S.A. (2009) Loss of inhibin alpha uncouples oocyte-granulosa cell dynamics and disrupts postnatal folliculogenesis. *Dev. Biol.*, **334**, 458–467.
55. Haavisto, A.M., Pettersson, K., Bergendahl, M., Perheentupa, A., Roser, J.F. and Huhtaniemi, I. (1993) A supersensitive immunofluorometric assay for rat luteinizing hormone. *Endocrinology*, **132**, 1687–1691.
56. Naillat, F., Prunskaite-Hyyrylainen, R., Pietila, I., Sormunen, R., Jokela, T., Shan, J. and Vainio, S.J. (2010) Wnt4/5a signalling coordinates cell adhesion and entry into meiosis during presumptive ovarian follicle development. *Hum. Mol. Genet.*, **19**, 1539–1550.
57. Tomizawa, S., Kobayashi, H., Watanabe, T., Andrews, S., Hata, K., Kelsey, G. and Sasaki, H. (2011) Dynamic stage-specific changes in imprinted differentially methylated regions during early mammalian development and prevalence of non-CpG methylation in oocytes. *Development*, **138**, 811–820.
58. Heikkila, M., Prunskaite, R., Naillat, F., Itaranta, P., Vuoristo, J., Leppaluoto, J., Peltoketo, H. and Vainio, S. (2005) The partial female to male sex reversal in wnt-4-deficient females involves induced expression of testosterone biosynthetic genes and testosterone production, and depends on androgen action. *Endocrinology*, **146**, 4016–4023.
59. Wang, F., Flanagan, J., Su, N., Wang, L., Bui, S., Nielson, A., Wu, X., Vo, H., Ma, X. and Luo, Y. (2012) RNAscope: a novel in situ RNA analysis platform for formalin-fixed, paraffin-embedded tissues. *J. Mol. Diagn.*, **14**, 22–29.
60. Kainulainen, V., Sundvall, M., Maatta, J.A., Santiestevan, E., Klagsbrun, M. and Elenius, K. (2000) A natural ErbB4 isoform that does not activate phosphoinositide 3-kinase mediates proliferation but not survival or chemotaxis. *J. Biol. Chem.*, **275**, 8641–8649.